Construction and Building Materials 274 (2021) 122097

Contents lists available at ScienceDirect

Construction and Building Materials

journal homepage: www.elsevier.com/locate/conbuildmat

The chloride-induced corrosion of a fly ash concrete with nanoparticles and corrosion inhibitor

Manu Harilal [a], Deepak K. Kamde [b], Sudha Uthaman [b], R.P. George [a,*], Radhakrishna G. Pillai [b], John Philip [a], Shaju.K. Albert [a]

[a] Corrosion Science and Technology Division, MCG, Metallurgy and Materials Group, Indira Gandhi Centre for Atomic Research, HBNI, Kalpakkam, Tamil Nadu 603102, India
[b] Department of Civil Engineering, Indian Institute of Technology Madras, Chennai 600 036, India

HIGHLIGHTS

- Corrosion resistance of steel rebar in a ternary concrete (CFNI) is investigated.
- Chloride resistance and corrosion inhibition of CFNI is studied.
- Apparent diffusion coefficient was found to be one order less in CFNI concrete.
- Significantly lower chloride ingress rate is seen in CFNI concrete.
- CFNI concrete is a promising concrete mix for improving service life.

ARTICLE INFO

Article history:
Received 11 September 2020
Received in revised form 27 November 2020
Accepted 17 December 2020
Available online 29 December 2020

Keywords:
Fly ash concrete
Reinforcement
Nanoparticles
Corrosion inhibitor
Service life

ABSTRACT

The urge to reduce the carbon footprints from cement production warrants the development of more sustainable approaches in the construction industry. Towards this, the long term corrosion resistance of the embedded steel rebar in a novel ternary-blended reinforced concrete system with 56 wt% Ordinary Portland cement (OPC), 40 wt% fly ash, 2 wt% nanomodifiers, and 2 wt% corrosion inhibitor (referred to as CFNI) was studied by chemical and electrochemical tests in a simulated chloride environment for 180 days. The performance was compared with three other concrete systems (CC (100% OPC), CF (60 wt% OPC and 40 wt% fly ash) and CFN (58 wt% OPC, 40 wt% fly ash and 2 wt% nanomodifiers). The electrochemical results indicated a significant enhancement in the corrosion resistance of steel in the CFNI concrete as compared to other systems. A five times higher value of polarization resistance (R_p) is obtained in CFNI, as compared to the control concrete, indicate the better resistance of CFNI. Further, in CFNI specimen, the chloride ingress rate was significantly lower and the Field Emission Scanning Electron Microscopy (FESEM) images showed no microcracks or pores at the corroded concrete-steel interface of CFNI specimens. The apparent diffusion coefficient (D_{cl}) of the concrete system was determined using the bulk diffusion test and chloride profiling. The value of D_{cl} for CFNI concrete was found to be one order less in magnitude than other concrete specimens, indicating the enhanced resistance against chloride attack. These results show that CFNI concrete is a promising ternary-blended concrete mix to achieve long corrosion-free service life for the structures in aggressive chloride environments.

1. Introduction

The continuously increasing boom in urbanization and infrastructure development increases the demand for cement [1]. The production of Ordinary Portland Cement (OPC) results in carbon emission which is reported to be 7% of the global carbon emission [2]. This may have significant adverse effects on the global environment and the sustainability of concrete construction [3]. One of the techniques to facilitate sustainable concrete construction is to partially replace cement by using minerals like silica fume, fly ash, and ground granulated blast furnace slag which are called supplementary cementitious materials (SCMs) [4-6]. Despite the significant advancements in the field of construction materials (i.e., use of various chemical admixtures and SCMs, low water-binder ratio, etc.), many concrete structures continue to suffer from inadequate corrosion-free service life, especially when located in marine and coastal regions with severe chloride conditions [7]. This leads to many infrastructures warranting repair within ten years of service

* Corresponding author.

https://doi.org/10.1016/j.conbuildmat.2020.122097
0950-0618/

life due to corrosion of reinforcement [8]. This deterioration is more pronounced in chloride environments [9,10]. The premature deterioration of structures can result in a large number of repair of RC structures and repetitive repairs [11]. Therefore, there is a need to develop quality concretes with adequate resistance to chloride penetration and other forms of degradation.

Many studies reveal that the propagation time for corrosion is significantly shorter than the initiation time [12-14]. Therefore, extensive investigation on steel–concrete interface properties and concrete transport properties is warranted to achieve the desired service life of concrete structures [15]. To augment the service life, the most sustainable way is to reduce the rate of diffusion of chlorides into concrete [16,17].

During the diffusion of chloride ions, they can bind with the hydration products or remain as free ions in the concrete pore solution [18]. These free chloride ions diffuse further into concrete due to the concentration gradient [19]. The chloride binding initiates the formation of Friedel's salt (FS), resulting in a reduction in the rate of chloride transport [18,20,21]. Hence, the capability of concrete to resist the chloride attack is measured based on its capacity to bind chloride ions (i.e., resistance to chloride transport); and also measured as the apparent diffusion coefficient [22]. Several chloride binding mechanisms involve the chloride binding chemical reaction occurring between the chloride ions and the hydration products such as C_3A (tricalcium aluminate) and C_4AF (tetracalciumalumino ferrite), that result in the formation of Friedel's salt ($3CaO{\cdot}Al_2O_3{\cdot}CaCl_2{\cdot}10H_2O$) [18,21]. FS is stable in basic solutions, but becomes unstable at lower pH values as in the case of carbonated concrete [23,24].

Many reports suggest that concrete offers more resistance to chloride penetration upon the use of supplementary cementitious materials (SCMs) like fly ash [25,26]. However, fly ash incorporated concrete possess some drawbacks such as high levels of calcium leaching, delayed setting and lower initial strength [27]. These limitations can be overcome by incorporating nanoparticles such as nano-$CaCO_3$, nano-TiO_2, nano-SiO_2, etc. [28]. The combined use of nano-TiO_2 and nano-$CaCO_3$ can dramatically enhance the properties of fly ash modified concrete, as reported by Uthaman et al. [29]. It has also been established that nanoparticles help in improving the resistance against the initiation and propagation of corrosion of rebars embedded in concrete [30,31].

Another approach to increase the resistance against chloride transport is to use corrosion inhibitors due to their advantages, such as convenience, cost-effectiveness, availability and high corrosion resistance. It has been reported that corrosion inhibiting admixtures can increase the resistance to chloride penetration and reduce the critical chloride threshold [32]. Corrosion inhibitors are added into concrete either during mixing or application on to the external surface of hardened concrete [33]. The application of corrosion inhibitors like calcium nitrite, sodium nitrite, and potassium chromate in concrete has been widely investigated [34,35]. It is reported that sodium nitrite is an effective corrosion inhibitor for rebars in the presence of chloride ions, but has adverse effects on the concrete strength [36,37]. A subsequent study shows that an adequate dosage of sodium nitrite based inhibitor improves the corrosion resistance of the reinforcing steel without any adverse effect on the compressive strength [38].

According to NACE Impact Report, nearly 50% of concrete structures hit a major repair within 10 years of service [8]. The costs of addressing corrosion are estimated to be about 3–4% of the GDP of the developed nations. This warrants the need for the development of quality concrete with improved corrosion resistance for enhanced service life and savings on corrosion cost. The partial replacement of cement with supplementary cementitious materials (SCMs) like fly ash helps to achieve sustainability and improves the corrosion resistance of concrete. The addition of nanoparticles and corrosion inhibiting admixtures are also shown to increase the resistance to chloride penetration and reduce the critical chloride threshold. There are no studies reported so far on the combined effect of fly ash, nanoparticles and corrosion inhibitor in improving the corrosion resistance of steel rebars in reinforced concrete structures. We try to bridge this gap through this systematic study using a concrete mix involving a combination of OPC, fly ash, nanoparticles and corrosion inhibitor to evaluate the synergic effect of the additives in improving the concrete properties.

As per the government initiative to reduce carbon footprint, we developed a ternary blended high performance green concrete (CFNI), with a combination of 56 wt% OPC, 40 wt% fly ash, 2 wt% nano-$CaCO_3$ and nano-TiO_2 (1:1 ratio) and 2 wt% $NaNO_2$ based anodic mixed inhibitor solution [39]. The anti-microbial and anti-fungal resistance of the CFNI concrete composition was investigated in our previous studies and the results were highly encouraging with CFNI concrete exhibiting enhanced properties [40,41]. This paper focuses on the chloride-induced corrosion of the embedded steel rebar inside reinforced CFNI concrete and the improvement in the corrosion resistance, if any, due to the additives are discussed in detail. The results of the present study together with the previous results can be used to determine the potential of CFNI concrete in an aggressive marine environment where corrosion due to chlorides and microorganisms are inevitable.

2. Experimental program

2.1. Materials and mix proportion

Table 1 shows the chemical composition and physical properties of cement (as per ASTM C150) and ASTM class F- siliceous type fly ash used in the present study. Crushed black granites of 12 mm and 20 mm size were used as the coarse aggregate and natural river sand of size less than 4.75 mm was used as the fine aggregate. Table 2 provides the properties of the aggregates. Potable water was used for making the specimens. The superplasticizer used was sulphonated naphthalene based high range water reducing admixture conforming to ASTM C494 type F [42]. Commercial laboratory-grade nano-anatase TiO_2 and nano-$CaCO_3$ with an initial particle size of 400–500 nm (as per the manufacturer) were used. The nanoparticles were reduced to 20–70 nm size by mechanical alloying and the detailed procedure is reported in our previous study [39]. Commercially available dark brown sodium nitrite based anodic mixed inhibitor solution of relative density 1.16 and pH 11.1 was used as the corrosion inhibitor in this study. The cement, fly ash, sand and coarse aggregates were thoroughly mixed in a laboratory counter current mixer. The nanoparticles and inhibitor were added into the potable water before mixing with the mixture.

Four types of M45 grade concrete compositions (corresponding to a target compressive strength of 45 MPa at the age of 28 days) were designated and fabricated as follows: (i) CC – Conventional Concrete with M45 grade and 100% OPC; (ii) CF – Concrete with 60 wt% OPC and 40 wt% fly ash, (iii) CFN – Concrete with 58 wt% OPC, 40 wt% fly ash and 2 wt% nanophase modifiers (1 wt% nano-anatase TiO_2 and 1 wt% nano-$CaCO_3$); (iv) CFNI – Concrete with 56 wt% OPC, 40 wt% fly ash, nanophase modifiers and corrosion inhibitors (1 wt% nano-$CaCO_3$, 1 wt% nano-TiO_2, and 2 wt% $NaNO_2$ inhibitor). The detailed mix designs used for casting the concrete specimens are shown in Table 3. The total volume of cementitious materials in all the specimens was 450 kg/m^3. The water-to-cement ratio of all the specimens was fixed by keeping a constant target slump of 100 mm.

Table 1
Chemical composition and physical properties of cement and fly ash used in this study.

Oxides	Concentration (wt. %)			Properties	
	(OPC)	Class F Fly ash		(OPC)	Class F Fly ash
CaO	62.7	0.68	Fineness (Blaine's Permeability in m^2/kg)	320	343
SiO_2	21	59.3	Normal consistency (%)	27	27.5
Al_2O_3	5.9	35.2	Specific gravity	3.14	2.05
Fe_2O_3	4.6	2.87	Soundness (mm)	2	1.3
MgO	1.6	0.24	Lime reactivity (MPa)	–	5.3
SO_3	1.5	0.28			
Loss on ignition	2.8	0.17			

Table 2
Properties of coarse and fine aggregates.

Properties	Fine aggregates	Coarse aggregates
Specific Gravity	2.83	2.85
Fineness Modulus	2.84	–
Water Absorption	0.51%	0.55%
Bulk Density	16.7 kg/m^3	16.4 kg/m^3

2.2. Specimen preparation

Three replica cylindrical reinforced concrete specimens with 110 mm height and 70 mm diameter were fabricated for all four types of systems. Fig. 1 shows the schematic diagram of the test specimen used for the electrochemical measurements. At the centre of each specimen, Quenched and Self-Tempered (QST) steel rebars of 100 mm length and 12 mm diameter were placed such that it gives a clear concrete cover of 25 mm from all the sides. The rebars were cleaned in the pickling solution (500 ml conc. HCl, 500 ml distilled water and 3.5 gm of hexamine), cleaned with acetone, washed with distilled water, and then dried before embedding them in concrete. The bottom surfaces of the rebars were sealed with two layers of epoxy coating. Table 4 shows the chemical composition of the steel rebar used in the study. Electrical connections were made with the help of copper wires connected to the uncoated end of the rebar by the process of brazing. These arrangements were mechanically vibrated and compacted using a table vibrator.

The specimens were cured in the mould for about 24 h. Then, they were removed from the mould and moist cured in water at ambient temperature under laboratory conditions (27 ± 5 °C and 65 ± 5% relative humidity (RH)) for 28 days. Then, the top and bottom surfaces of the specimens were coated with an epoxy resin to restrict the transport of chloride ions through the surface of cylindrical specimens. The concrete specimens were then immersed in a 3.5% NaCl solution to mimic the marine environment under accelerated conditions [16]. The specimens were exposed to 15-days wet and 15-days dry cyclic regime in NaCl solution for 180 days.

2.3. Depth of chloride ion penetration

The surface chloride concentration (C_s) increases with the exposure time [43-45]. Therefore, maximum surface chloride concentration (C_{max}) can be determined after long-term exposure (say, several years) of the concrete specimen to the chloride-rich environment. However, such long exposure may not always be possible. Therefore, in this study, rapid migration tests (i.e., NT-build 492) were conducted on concrete test specimens. Three replica concrete cubes of size 150 × 150 × 150 mm were cast and moist cured for 28 days at a room temperature of 28 ± 2 °C. Later, cylindrical concrete cores were extracted from these specimens and cut to 50 mm length. After that, the specimens were dried and coated with a waterproofing material on curved surfaces, leaving the top and bottom surfaces free. Fig. 2a shows the experimental setup used for the migration test.

Migration test was performed as per NT-build 492 [46]. After the completion of the migration test, the cylindrical specimens were broken into halves. Then, silver nitrate solution was sprayed on the freshly fractured surfaces and the depth of the white precipitate of AgCl formed at the fractured surface indicates the depth of chloride penetration. The more the depth of chloride penetration, the less the chloride resistance. The average chloride concentration of the 5 mm thick concrete layer in contact with the chloride solu-

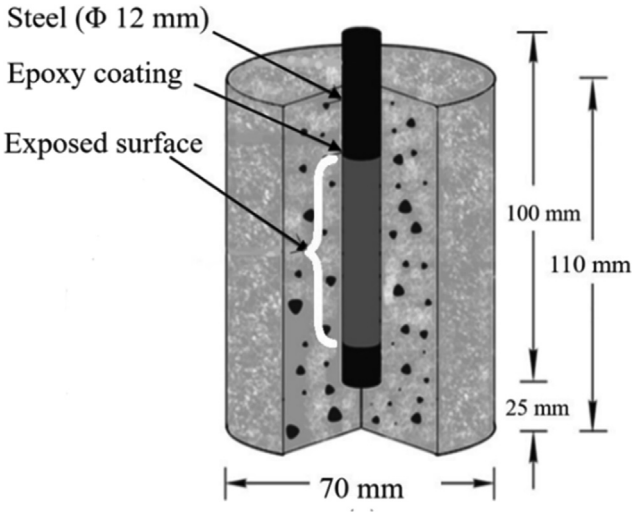

Fig. 1. Schematic view of the cylindrical reinforced concrete specimens used for the electrochemical measurements.

Table 3
Mixture proportion for the various concrete systems.

Concrete type	Cement (kg/m^3)	Fly Ash (kg/m^3)	F. Agg. (kg/m^3)	C.Agg. (kg/m^3)	TiO_2 (kg/m^3)	$CaCO_3$ (kg/m^3)	Inhibitor (kg/m^3)	water (kg/m^3)	Superplasticizer (kg/m^3)	Water-binder ratio
CC	450	–	797	1090	–	–	–	166.5	3.6	0.37
CF	270	180	744	1017	–	–	–	171	4.5	0.38
CFN	261	180	733	1010	4.5	4.5	–	162	5.4	0.36
CFNI	252	180	724	1003	4.5	4.5	9.0	144	5.4	0.32

Table 4
Chemical composition of Fe500 TMT steel rebar used as reinforcements for the electrochemical test specimens (wt. %).

C	Si	V	P	S	Mo	Nb	Fe
0.24	0.06	0.028	0.039	0.030	0.09	0.023	Balance

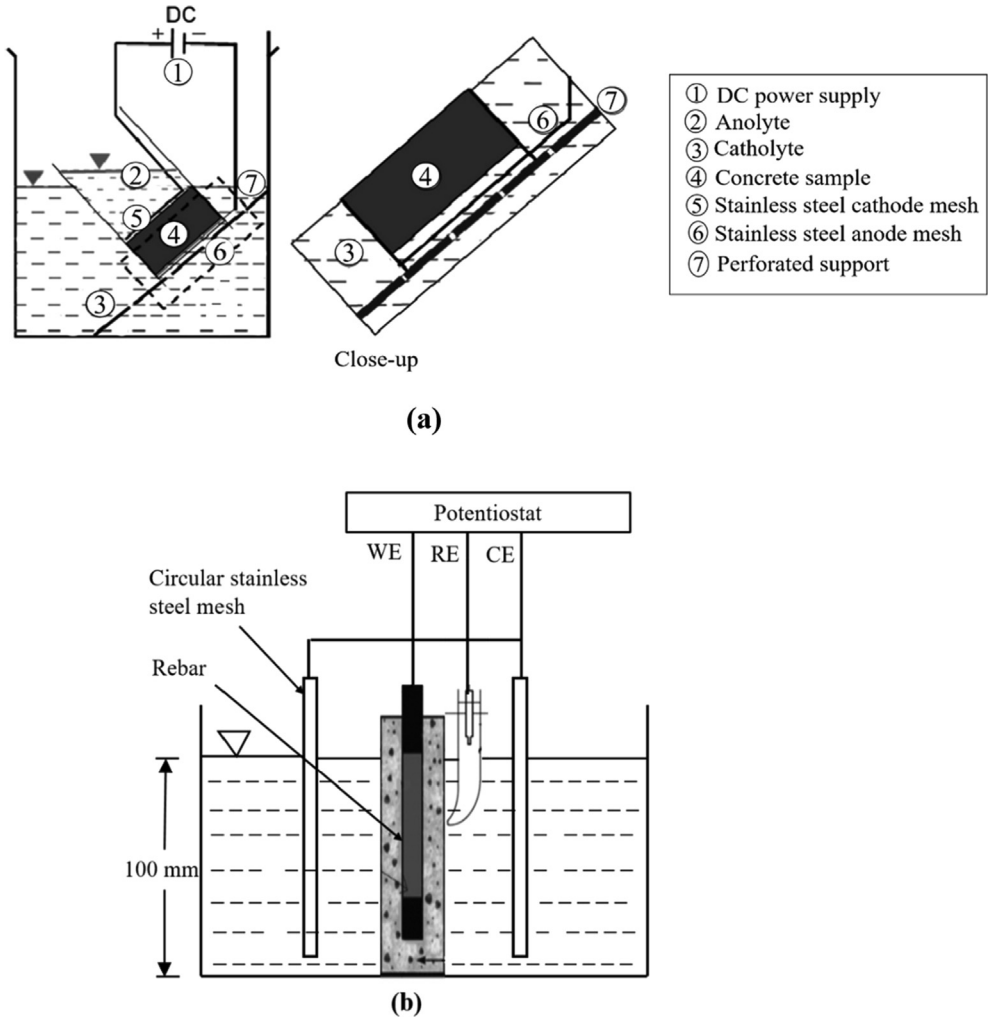

Fig. 2. (a) Schematic view of accelerated chloride migration test setup (NT build 492 (2011)) (b) schematic view of the experimental set up used for the electrochemical measurements.

tion (during the migration test) was determined and is defined as C_{max}.

2.4. Apparent chloride diffusion coefficient of concrete (Dcl)

To determine the apparent chloride diffusion coefficient for the different concrete compositions, the bulk diffusion test was performed on 100 × 200 mm long cylindrical concrete specimens. The specimens were cured for one year to limit the influence of microstructure evolution on the rate of chloride ingress. After curing, the cylinder specimens from each concrete composition were sliced into two samples of 50 mm thickness. The specimens were then coated with epoxy and kept for hardening. After the epoxy has hardened, the slices were conditioned with a saturated calcium hydroxide solution and immersed in 2.8 M NaCl solution for 56 days as per ASTM C1556 [47]. Chloride profiles up to 25 mm were obtained for each specimen by grinding using a lathe machine and single head diamond dresser tools. The powdered samples from each layer were collected and chloride concentrations were determined as per SHRP-S-330 [48]. Later, these chloride profiles and Fick's second law (Equation (1)) were used to determine the D_{cl}.

$$C(x,t) = C_s - (C_s - C_i) \times erf\left(\frac{x}{\sqrt{4 \times D_{cl} \times t}}\right) \quad (1)$$

where, $C(x, t)$ is the chloride concentration measured at depth 'x' from the exposed concrete surface at an exposure time of t s, 'C_s' is the surface chloride concentration built-up on the exposed concrete surface after exposure time t seconds, 'C_i' is the initial chloride concentration (assumed to be zero in this study), 'D_{cl}' is the apparent chloride diffusion coefficient, and (erf) is the error function. Here, D_{cl} is considered as a time-variant function and determined by using Equation (2),

$$D_{cl}(t) = D_{cl} \times \left(\frac{t_0}{t}\right)^m \quad (2)$$

where, $D_{cl}\ (t)$ is the apparent chloride diffusion coefficient at age t *days*, D_{cl} is the apparent chloride diffusion coefficient of concrete at the age of 28 days, 't_0' is equal to 28 days, t is the age of the specimen in days, and m is the decay constant/maturity coefficient, which was calculated using Equation (3) [49]. The relation was used to incorporate the effect of supplementary cementitious materials.

$$m = 0.2 + 0.4\left(\frac{\%\ of\ flyash}{50}\right) \tag{3}$$

where, m is the decay constant, % of fly ash is the percentage replacement with OPC. For concrete with nanomaterials and inhibitors, 'm' value used is 0.6, which is the maximum decay constant allowed [50].

2.5. Electrochemical measurements in simulated chloride environment

2.5.1. Linear polarization resistance (LPR) technique

Fig. 2b shows the schematic diagram of the experimental setup used for the measurements of resistance to polarization (R_p) of the steel–concrete test specimens using a three-electrode arrangement. Here, the rebar is the working electrode, Ag/AgCl is the reference electrode, and circumferentially placed stainless steel is the counter electrode. There are some uncertainties associated with LPR measurements due to the ohmic (IR) drop resulting from the electrical resistivity of concrete and the distance between embedded rebar and reference electrode. This IR drop during the time of electrochemical measurements on rebars originates from the flow of current through the finite resistivity of reinforced concrete. The corrosion measurements carried out without considering the IR drop lead to too small corrosion density (i_{corr}) values [51]. In this study, the reference electrode was placed very near to the rebar during the measurements to minimize the measurement errors.

The open circuit potentials of three replica specimens were measured using ACM Galvo Gill Electrochemical Workstation (Gill 12, M/s ACM instruments, UK) as per ASTM G59-97 [52] after immersion in 3.5% NaCl solution for 55 min and averaged at the end of each cycle during the exposure period of 180 days. To accelerate the chloride transport through the concrete, all the test specimens were subjected to alternate wetting and drying cycles. One cycle consists of 15 days of wetting in NaCl solution, followed by another 15 days of drying in the open air for a total period of 180 days. The application of drying and wetting cycles accelerate corrosion by creating nucleating paths during the drying cycle which enables easy penetration of chlorides into the concrete and breaking the stable passive film over the steel rebars [53]. The instantaneous corrosion rates of the reinforcing steel in concrete were then measured at the end of each cycle, by linearly polarizing them from its equilibrium potential (OCP) value to ±25 mV, to ensure that for active corrosion the potential shift lies within the linear Stern-Geary region [54]. The sweep rate adopted was 10 mV/min. The resulting LPR curve was obtained and the polarization resistance (R_P) was determined from the tangent at i = 0. The R_P value obtained was used for the calculation of the corrosion rate following ASTM G59- 97 (2014) [52]. The estimation of corrosion rate from polarization measurements requires the quantitative information about the Stern-Geary coefficient, B, which is 26 mV in the case of active corrosion and 52 mV in the case of passive corrosion for a reinforced concrete specimen [55]. In this study, the value of B was taken as 26 mV [53,56-58], with a maximum measurement error factor of 2 for the estimation of corrosion rates [55].

2.5.2. Gravimetric mass loss measurement and visual examination

The initial weights of the reinforcing steel rebars were measured before embedding them in concrete. The concrete specimens with embedded steel were immersed in a 3.5% NaCl solution and subjected to six alternate wetting and drying cycles for 180 days. After that, the concrete specimens were cut open, and the rebars were visually observed for the degree of corrosion. The rebars were then cleaned in a pickling solution (500 ml conc. HCl, 500 ml distilled water and 3.5 gm of hexamine) according to ASTM G1-90 [59]. The weight of the cleaned specimens was measured, and the loss in weight was calculated. The rates of corrosion were determined in millimeters per year (mmpy) using Eqn 4, where 87.6 is a conversion factor as reported in a previous study [60]:

$$\text{Corrosion rate (mmpy)} = \frac{87.6 \times weight\ loss\ (mg)}{density\ \left(\frac{g}{cm^3}\right) \times area\ (cm^2) \times time\ of\ exposure\ (h)} \tag{4}$$

2.5.3. Electrochemical impedance spectroscopy (EIS) measurement

Electrochemical impedance spectroscopic (EIS) measurements at open circuit potential were carried out using the same test setup as in the case of LPR measurements, with a computer-controlled potentiostat (PGSTAT30 Autolab, EcoChemie, Netherlands) in an alternating frequency range of 10 mHz to 100 kHz. AC signal with an amplitude of 10 mV was applied to the system, and the impedance and current values were measured using frequencies within the applied range. The impedance spectra were then analyzed by fitting the experimental data to the equivalent electrical circuit with the help of Z-View software.

2.5.4. Galvanic macrocell corrosion studies

Fig. 3 shows the photograph and schematic of the rectangular concrete prism specimens of size (220 mm × 152 mm × 110 m m) used for the galvanic macrocell corrosion studies. Two rebars of 12 mm diameter were placed at the bottom (cathode) and one rebar was placed at the top (anode), similar to the ASTM G109 (2013) specimen [61]. The anode-to-cathode ratio of the test specimens was 0.5 to induce accelerated corrosion. Concrete cover of 25 mm from the bottom and 20 mm from the top was maintained in all the replica. Electrical connections were made between the anode and cathodes using a 100 Ω resistor.

The rebars were cleaned with the pickling solution for 10 min, dried and cleaned by wire brush before embedding inside the concrete specimens. Thin epoxy based coating was applied on the 40 mm long region at both ends of the rebar and cured for two days. Concrete was poured into the moulds in three layers, compacted, consolidated and mechanically vibrated during casting of the specimens. Wood float finish was then given to the top concrete surface. The specimens were cured in the mould for one day followed by moist-curing for another 27 days. After curing, the four vertical sides of the concrete prism specimens were sealed with the epoxy based coating. All the concrete specimens were exposed to 3.5% NaCl solution immediately so that 200 mm length of steel rebar in concrete is exposed to chlorides. Then, the specimens were kept in the laboratory environment for 180 days and subjected to macrocell corrosion measurements under alternate wetting and drying cycles as in LPR, EIS and GML measurements.

The macrocell current flow between the anode and cathode was measured with the help of an auto-ranging high impedance digital voltmeter (M/s. Meco Meters Pvt Ltd., India), keeping Ag/AgCl as the reference electrode. The measurements were carried out under wet conditions once in every cycle. Tests were conducted on triplicate specimens for each concrete composition and the average values are recorded [13,62].

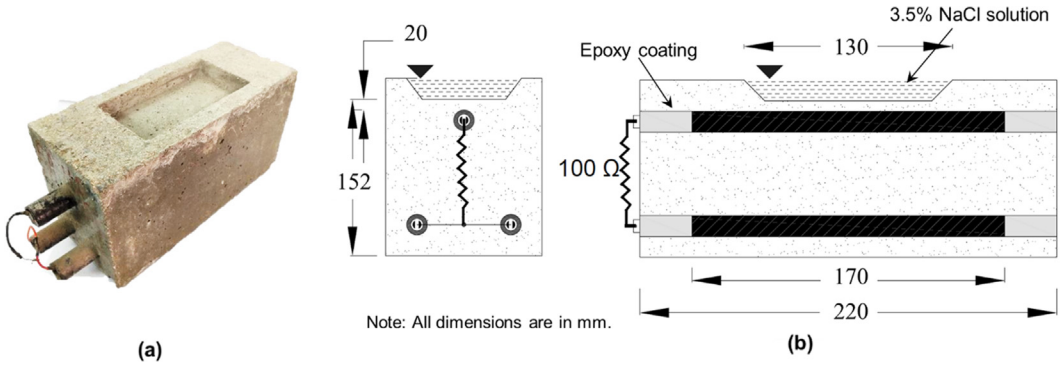

Fig. 3. (a) Photograph of the specimen and (b) schematic sketch of macrocell corrosion measurements used (ASTM G109-2013).

2.6. Preparation of powder aqueous solution from the corroded concrete-steel interface

After exposure to 3.5% chloride solution for 180 days, specimens were cut open, and concrete samples collected from surfaces near the top rebar from various concrete systems were powdered and stored in airtight plastic covers.

2.6.1. pH and conductivity measurements

A commonly used method to evaluate the pH of concrete is the analysis of pore water extracted out of concrete [63]. This method is adopted to measure pH of the various concrete systems. The concrete samples were initially powdered using mechanical means and then finely powdered using a mortar and pestle. These extracts were then passed through a sieve of 80 mm to obtain very finely ground particles. 5 g of this powder was mixed with 50 ml of doubly distilled water in a beaker and stirred thoroughly for 2 h using a magnetic stirrer. After 2 h, the solution was filtered and the pH and conductivity of this powder solution were measured using a portable pH meter (M/s. Hanna Instruments, Romania) and digital conductivity meter (M/s. HACH Company, USA), respectively. The concrete powder aqueous solution prepared from the samples has almost all the characteristics of the species in the near vicinity of the rebar in the contaminated concrete, which contains cement hydrates, coarse and fine aggregates, and chloride ions [64]. For each concrete system, three readings were recorded and the average values are reported.

2.6.2. Estimation of free chloride contents

The amount of free chloride ions present in the concrete pore solution was determined using the water-soluble extraction method [65]. The free chloride contents of the different concrete systems were measured using twenty ml of the filtered solution prepared from the powdered samples. The chloride content was determined with the help of a chloride measuring probe. Three readings were taken for each system and the average values were determined. The free chloride content in the samples was measured and expressed in g/l [25].

2.7. Morphological and chemical characterization of the corroded concrete-steel interface

2.7.1. FESEM analysis and elemental mapping

The concrete core samples were extracted from the near vicinity of the corroded rebars. The extracts were crushed into a very fine powder and pressurized under compression to form pellets. These test samples were placed in a vacuum desiccator until a constant weight is reached, and then coated with a thin gold layer to make it conductive using gold sputtering by a Magnetron Coating (MCM-100). The surface topography of the pellets from different concrete systems was then visualized using a Field Emission Scanning Electron Microscope (M/s. Carl Zeiss, Germany). For elemental analysis, Energy Dispersive Spectroscopy (EDS) associated with the SEM was used for mapping the distribution of elemental composition in the extracted test samples.

2.7.2. X-ray diffraction (XRD) analysis

The core samples extracted from the concrete-steel interface of various systems were crushed into small pieces with a mallet and then finely powdered using a mortar and pestle. The pulverized samples were then analyzed by powder X-ray diffraction method. The XRD analysis was conducted using an X-ray diffractometer (Inel – EQUINOX 2000 diffractometer) with an X-ray source of Co-Ka radiation (k = 1.7889 Å) over a 2θ range of 15°–90° at a scan step size of 0.05°. The X-ray tube voltage and current were fixed at 35 kV and 20 mA, respectively [39]. The phases involved in the diffraction spectrum were identified with the standard database (JCPDS database) for the X-ray powder diffraction pattern [66].

2.7.3. Thermogravimetric analysis for assessment of Friedel's salt and portlandite content

Thermogravimetric analysis (TGA) analysis was carried out using a Thermal Analysis SDT Q600 (USA make) instrument. The extracts from the concrete-steel interface of various systems exposed to 3.5% NaCl solution for 180 days were broken into small fragments and ground into a fine powder using a mortar and pestle after separating the fine aggregates. The powder samples were dried at 100 °C in an oven, cooled to room temperature and kept in a desiccator before TGA analysis [67]. A few milligrams of the samples were taken into a ceramic crucible and Al_2O_3 powder was used as reference material. The changes in the mass of the samples were measured after heating the powders from ambient temperature to 1000 °C at a heating rate of 10 °C per minute under a flowing nitrogen gas atmosphere.

The amounts of Friedel's salt (FS) and Portlandite ($Ca(OH)_2$) in the samples extracted from the concrete-steel interface is estimated based on the mass loss occurring between 230 and 410 °C [68] and 421–500 °C [69], respectively. The content of FS in the powder samples was determined according to the following equation:

$$m_{FS} = \frac{M_{FS}}{6 \times M_H} m_H \quad (5)$$

where m_{FS} is the mass fraction of FS in the sample (wt. %), m_H is the measured loss of water by TGA (wt. %), M_{FS} is the molar mass of FS (561.3 g/mol),and M_H is the molar mass of H_2O (18.02 g/mol) [70].

Similarly, the content of portlandite was quantified by determining the weight loss in the temperature range from 400 to 500 °C according to the equation:

$$m_{CH} = \frac{M_{CH}}{M_H} \times m \quad (6)$$

where m_{CH} corresponds to the mass fraction of portlandite in the sample (wt. %), m is the loss of water from portlandite (wt. %) in the temperature range, M_{CH} is the molar mass (74.09 g/mol) of portlandite, and M_H is the molar mass (18.02 g/mol) of H_2O [70].

2.7.4. Fourier Transform infrared (FTIR) spectroscopic analysis

The different functional groups corresponding to the hydration products in the hardened concrete were determined with Fourier Transform Infrared (FTIR) spectroscopy. The FTIR spectrum of the concrete powders was collected using an infrared spectrometer (M/s. Bruker, Germany) in the transmission mode. The pellets for the characterization were prepared by mixing 3 mg of the concrete powder with 250 mg of potassium bromide (KBr). Sixteen scans were recorded in the range of 4000 cm^{-1} to 400 cm^{-1}.

2.8. Estimation of service life

In this study, the probabilistic service life of the reinforced concrete systems was estimated based on the time taken for the initiation of rebar corrosion. A MATLAB program (SL-chlor) developed by Rengaraju (2019) was used to estimate the service life [71]. SL-Chlor program considers the one-directional diffusion of chloride as per Fick's second law of diffusion (see Eq. (1)). Following input parameters were used for the estimation: Cs, C_{max}, D_{cl}, m, and Cl_{th}. The input parameters used in this study was determined using experiments in this study and from the field investigation of a 6-year old bridge structure presented in a previous work [13]. For probabilistic estimation of service life, 1000 number of simulations are considered. A probabilistic response was obtained and 50% of probability of initiation of corrosion was considered to be the end of service life [72].

3. Results and discussion

3.1. Depth of chloride ion penetration

Fig. 4a shows the average depth of chloride ion penetration in CC, CF, CFN, and CFNI concretes, estimated after the ingress of chloride ions using the chloride migration test. The depth of penetration in CC, CF, CFN, and CFNI was found to be 23, 11, 8, and 6 mm, respectively. It is seen that the chloride penetration in concrete with fly ash is reduced to 50% of the original value. Likewise, chloride penetration is found to be significantly decreased after the addition of nanoparticles, which is attributed to the denser microstructure due to the filler effect of nanoparticles. Further, the addition of inhibitor also increases the chloride resistance but it was not significantly visible in the fractured concrete piece shown in Fig. 4a. This may be because of the migration of charged ions of the inhibitor when potential is applied across concrete specimens during the migration test. These ions may not diffuse when concrete is exposed to the natural environment. Therefore, the depth of penetration in the case of CFNI is an overestimated one due to the fact that inhibitors were not effective due to the application of the potential [14].

Fig. 4b shows the results of the chloride migration test used to obtain a quantitative measure of the resistance against chloride ingress. The parameter obtained is the non-steady state migration coefficient which represents the rate of chloride ingress upon application of a potential. It can be seen that the value of the migration coefficient in CC specimens was 3.43 × 10^{-12} m^2/s. The addition of fly ash lowers the chloride migration coefficient of CF specimens to the order of 0.96 × 10^{-12} m^2/s (~72% compared to CC). The incorporation of nanoparticles further reduced the migration coefficients of CFN specimens to 0.73 × 10^{-12} m^2/s (~78% compared to CC). However, upon addition of inhibitor, the migration coefficient increased to a value of 1.16 × 10^{-12} m^2/s for CFNI specimens. It is reported that when inhibitors are used, they have additional ions. Thus, when a potential gradient is applied, these additional ions of inhibitors cause additional ionic flow [14]. This will result in an increase the value of the migration coefficient of CFNI than CFN. Therefore, the value for CFNI is not correct and it has to be validated using the Diffusion coefficient. The improved performance of CFNI due to chloride binding is observed during the long-term chloride diffusion test (See Section 3.2).

3.2. Chloride diffusion coefficients of concrete

Fig. 5 shows the chloride content profiles of the concrete samples obtained from CC, CF, CFN, and CFNI concrete specimens determined using SHRP-S-330. These chloride profiles were fitted using Fick's second law to determine the D_{cl} for each specimen. D_{cl} for CC, CF, CFN, and CFNI was found to be 3.17, 1.9, 1.11 × 10^{-11} m^2/Sec, and 8.56 × 10^{-12} m^2/Sec, respectively. Thus, D_{cl} for CFNI type of concrete was found to be one order less than other types of concrete specimens, indicating that the combination of nanomaterial and inhibitor can resist or lower the chloride ingress. Also, the chloride concentration on the surface of CFN and CFNI types of concrete is significantly higher than that on CC and CF surfaces as seen in Fig. 5. The accumulation of higher chloride concentration indicates the higher chloride binding capacity of the concrete with nanomaterials and inhibitor. Thus, the chloride ingress resistance for these concretes are ranked as CFNI > CFN > CF > CC.

3.3. Electrochemical measurements in the simulated chloride environment

Fig. 6a shows the variations in the open circuit potential values of reinforcement, measured with the LPR test before and after the alternate wetting and drying cycle in all four types of concrete test specimens. The extent of corrosion activity in the embedded rebars was determined as per ASTM C 876–09 [73]. Initially, the potential values of reinforcement in CC, CF and CFN specimens were in the range of −110 to −160 $mV_{Ag/AgCl}$ electrode, which is more negative than −105 $mV_{Ag/AgCl}$, indicating an uncertain probability of corrosion at the rebar level [73]. The rebar inside CFN concrete system showed a potential value of −92 mV, which is more positive than −105 $mV_{Ag/AgCl}$, indicating 10% probability of corrosion [73]. After 180 days of wet and dry exposure, the potential of CC specimens was found to be more negative than −255 $mV_{Ag/AgCl}$ indicating a 90% probability of active corrosion whereas, the rebars embedded in CF, CFN and CFNI test specimens showed potential values between −255 $mV_{Ag/AgCl}$ and −105 $mV_{Ag/AgCl}$, indicating an uncertain probability of corrosion [74].

In the case of CC specimens, the permeability and pore characteristics is comparatively on the high side [39] and hence more amount of chloride ions penetrated from the initial day of exposure and shifted the potential towards a negative direction [54]. Shaikh et al. [67] have reported that the addition of nano-$CaCO_3$ and fly ash together in conventional concrete could provide better corrosion protection to fly ash concrete. The addition of nano-$CaCO_3$ fills up the pores near the cement particles thereby reducing the porosity and permeability of the concrete specimens [75]. Incorporation of nano- TiO_2 up to 1.5 wt% can also act as filler, increases the rate of hydration and improves the corrosion resistance of the reinforc-

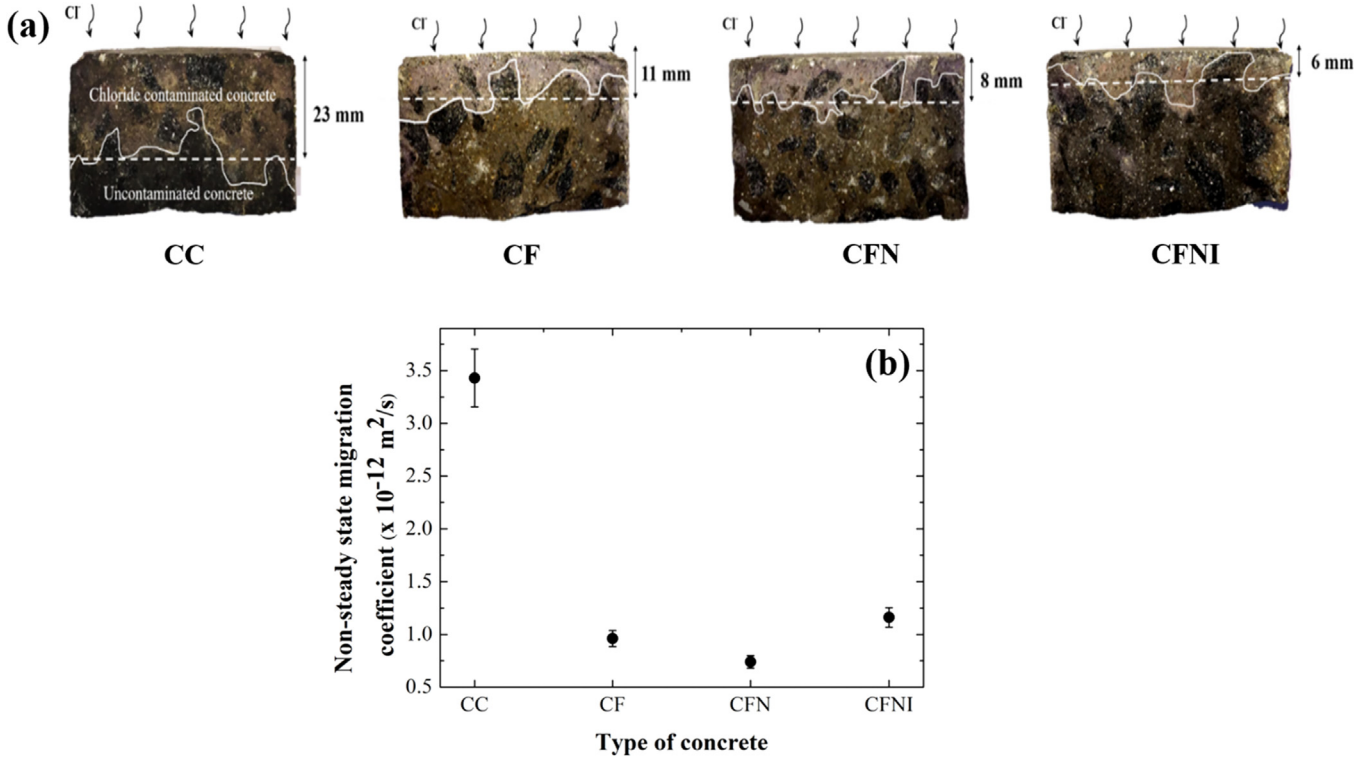

Fig. 4. (a) Average depth of chloride penetration measured using silver nitrate spraying for various concrete specimens and (b) estimated non-steady state chloride migration coefficient of different concrete systems using NT build 492.

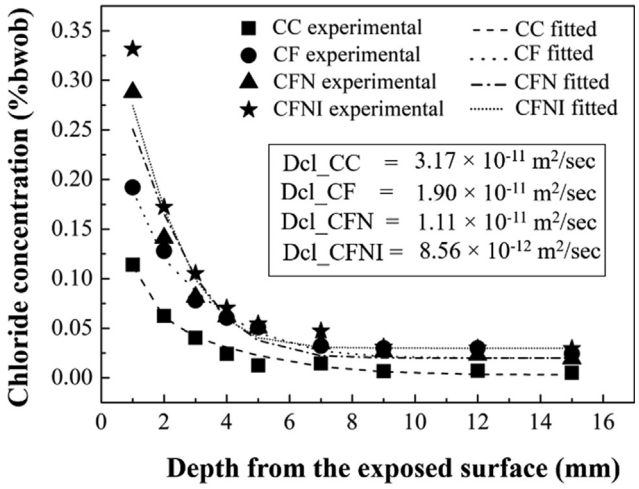

Fig. 5. Chloride content profile of different concrete specimens after 56 days of exposure in 3.5% NaCl solution determined using SHRP-S-330 (a) CC (b) CF (c) CFN and (d) CFNI.

ing steel [76]. Nguyen et al. [77] found that the amount of nanomaterials (1% by weight of cement) plays a major role in improving the chloride penetration resistance. When a combination of OPC, fly ash, 1 wt% nano-TiO_2, 1 wt% nano-$CaCO_3$ was formulated (CFN), the corrosion resistance of the reinforcing steel was enhanced because of the combined effect of the additives. The addition of sodium nitrite based corrosion inhibitor to this formulation (CFNI) ennobled the corrosion potential as compared to CC and CF specimens, but little lower than the nano-modified specimens.

The changes in the corrosion current density (i_{corr}) values of different concrete systems as a function of the exposure time, measured with the LPR technique is shown in Fig. 6b. During the initial exposure period, the CC specimens showed a comparatively higher i_{corr} value of 3.159 μA/cm^2. The modified concrete systems exhibited a reduction in the i_{corr} value corresponding to 1.158 μA/cm^2 in CF specimens, 0.118 μA/cm^2 in CFN and 0.321 μA/cm^2 in CFNI concrete system. The i_{corr} values showed a continuously increasing trend with the time of exposure in the electrolyte. After 180 days of exposure, the i_{corr} value is observed to be 18.2 μA/cm^2 in CC specimens, 3.02 μA/cm^2 in CF specimens, 1.27 μA/cm^2 in CFN specimens and 1.42 μA/cm^2 in CFNI specimens. According to Bavarian et al. [78], if the i_{corr} value measured is between 2.7 and 27 μA/cm^2 (moderate severity region), the corrosion damage can be expected in 2 to 10 years. In our study, both CC and CF specimens exhibited i_{corr} values in this range and hence is susceptible to failure within a short period. However, i_{corr} values between 0.5 and 2.7 μA/cm^2 correspond to low severity region and corrosion damage can be expected in these structures within 10–15 years. Both CFN and CFNI specimens showed i_{corr} values within this limit and thus, the addition of nanoparticles and inhibitor enables an extended service life for reinforced concrete structures.

Table 5 summarizes the final calculated values of LPR measurements on the different steel rebars in various concrete systems after 180 days of exposure in 3.5% NaCl solution. The highest corrosion potential (E_{corr}) value was observed in CC specimens (−378 mV) and CFN specimens showed the lowest (−88 mV). It is also understood that the resistance to polarization (R_p) values for the reinforcements embedded in CFN, and CFNI type specimens were higher than the R_p of steel embedded in CF and CC specimens. This R_p is used to calculate the rate of corrosion (i_{corr}) and is compared with the standard values reported [79]. The R_p values for CFN and CFNI specimens were 20,420 and 18292 Ω.cm^2, respectively which was found to be 13–14 times better than the CC specimens. CF specimens also showed a R_p value of 8636 Ω.cm^2, which was six

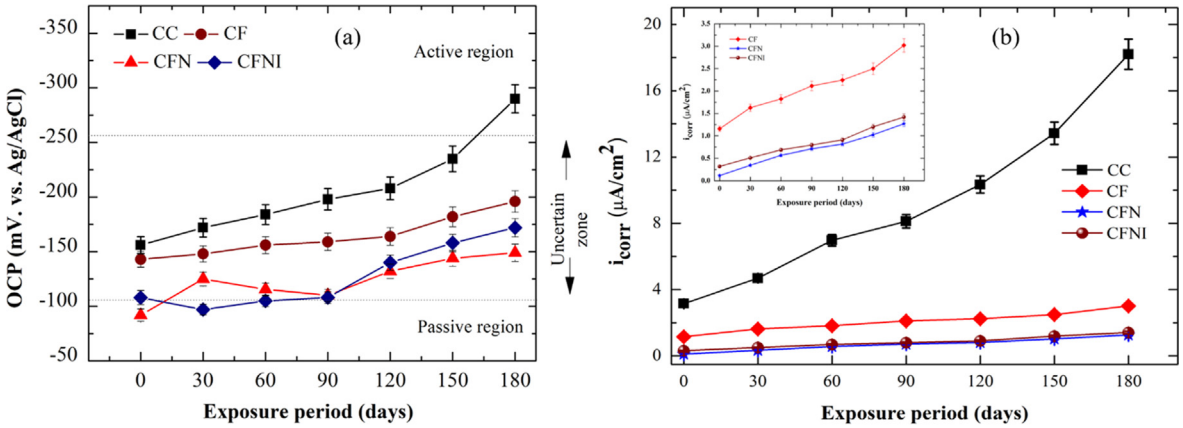

Fig. 6. (a) Open circuit potential of steel (b) evolution of i_{corr} in different concrete systems (CC, CF, CFN and CFNI) as a function of exposure period for 180 days in LPR test.

Table 5
Corrosion rate calculated from LPR technique for different concrete specimens after 180 days of exposure in 3.5% NaCl solution.

Type of specimen	Corrosion potential, E_{corr} (mV)	Polarization resistance, R_p ($\Omega.cm^2$)	Corrosion current density i_{corr} ($\mu A/cm^2$)	Corrosion rate (mmpy)
CC	−378	1433	18.20	0.23
CF	−185	8636	3.02	0.04
CFN	−88	20,420	1.27	0.02
CFNI	−110	18,292	1.42	0.02

times higher compared to CC specimens. The comparison indicated that the resistance against damage due to corrosion for modified concrete systems was around five times more than the control concrete.

The corrosion rates calculated from the LPR measurements are shown in Table 5**.** The highest corrosion rate of 0.23 mmpy was observed in CC specimens. This is because of the large number of pores present in OPC specimens, which allows the easy ingress of chloride ions. CF specimens showed a corrosion rate of 0.038 mmpy. It is reported that the filler effect of microparticles in fly ash and secondary hydration reaction result in the formation of calcium silicate hydrate (CSH) gels, which can enhance the properties of fly ash concrete [54]. The addition of nanoparticles and inhibitor was found to reduce the corrosion rate of both CFN and CFNI specimens to 0.016 and 0.018 mmpy, respectively, which is attributed to the improved pore structure [39].

Fig. 7a shows the average corrosion rates calculated in mmpy for the rebars embedded in the four types of concrete systems using gravimetric mass loss measurements. It can be observed that the corrosion rate for CC concrete system was the highest among all the concrete mixes (0.22 mmpy). This result was in agreement with the severe corrosion rate of rebar reported by Frolund et al. [80] using galvanostatic pulse technique. Any concrete with corrosion rates less than 0.22 mmpy is considered to improve the corrosion resistance of the embedded steel rebar. All the modified concrete systems showed corrosion rates less than 0.22 mmpy and were found to be in the low severity region according to Frolund et al. [80]. The CF specimens showed a corrosion rate of 0.07 mmpy, which means that the addition of fly ash improved the corrosion resistance of CF concrete system as a result of its pore filling effect during the process of cement hydration, thereby, producing an impermeable concrete with high alkalinity in the vicinity of

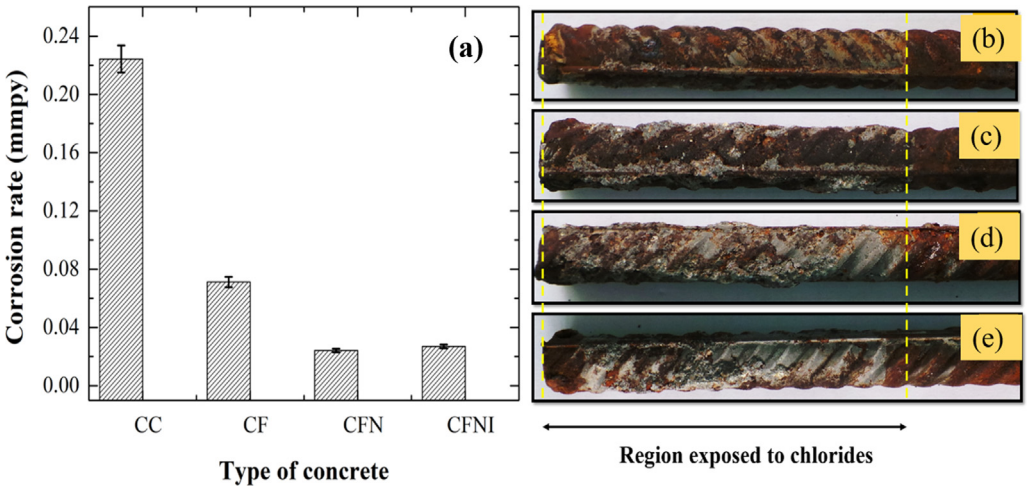

Fig. 7. (a) Average corrosion rate obtained using gravimetric mass loss (GML) measurements for steel and (b-e) photographs of the steel rebars (b) CC (c) CF (d) CFN (e) CFNI after the GML measurements in various concrete systems after 180 days of exposure in 3.5% NaCl solution.

rebar [25]. Harilal et al. [39] have reported that incorporation of nanoparticles and inhibitor can significantly decrease the chloride permeability of fly ash concrete. The corrosion rates of CFN and CFNI concrete specimens were 0.024 mmpy and 0.026 mmpy, respectively. The difference between the corrosion rates obtained from gravimetric mass loss and polarization experiments is due to the assumed measurement factor considered in the polarization experiments.

Fig. 7(b–e) shows the photographs of the steel rebars embedded inside various concrete systems after 180 days of exposure in 3.5% NaCl solution. The visual examination of the rebars showed that the one placed inside the CC specimen has undergone the maximum rusting. The adherence of concrete was visible on the rebars inside modified concrete specimens. This is in agreement with the studies conducted by Garcia et al. [81] and Bastidas et al. [82], where adherence of fly ash favoured stability to the rebars in aggressive chloride environments. The surface of CFN and CFNI specimens showed more adherence of concrete and hence the extent of rust formation was comparatively lesser in these specimens.

Fig. 8 shows the typical electrochemical impedance spectroscopy response from the steel concrete systems (CC, CF, CFN, and CFNI). The Nyquist plots for all the four specimens after 180 days of exposure in 3.5% NaCl solution recorded at room temperature (25 ± 2 °C) are shown in Fig. 8a. The data were fit using an electrical equivalent circuit (EEC) of the steel–concrete systems (Fig. 8c), which is similar to the reference [71] and Table 6 summarizes the corresponding best-fit parameters. The R_S is the resistance of solution, which is assumed to be constant in this study. R_C and CPE_C are the resistance and capacitance of concrete, respectively; $R_{S\text{-}C}$ and $CPE_{S\text{-}C}$ are the resistance and capacitance of steel–concrete interface, and R_{pf} and CPE_{pf} are the resistance and capacitance of passive film, respectively. It could be observed that with the addition of mineral admixtures and supplementary cementitious materials, resistance to corrosion improved (i.e., R_C (CF) > R_C (CC)). The R_C of CC and CF is significantly less than the R_C of CFN and CFNI. Note that the R_C (CFNI) < R_C(CFN). Though the resistance of concrete will help in reducing the rate of corrosion, it will not directly influence the resistance of initiation of corrosion. The information on resistance to initiation of corrosion can be extracted from the R_{pf} value of each element. Fitting of EIS response to EEC gave an R_{pf} (CFNI) value of $\approx 200 \times 10^4$ Ω.cm^2 > R_{pf} (CFN) $\approx 180 \times 10^4$ Ω.cm^2, indicating that the resistance of the passive film to initiation of corrosion for steel in CFNI concrete systems is higher than that in the CFN concrete system. The higher R_{pf} can be because of the denser passive film formed due to the presence of inhibitor [14].

Table 6
Best fitting results from the impedance spectra obtained after 180 days of exposure in 3.5% NaCl solution for all the four concrete systems.

Type of specimen	R_{pf} ($\times 10^4$ Ω.cm^2)	Error	χ^2
CC	10	2%	0.002
CF	15	6%	0.0002
CFN	180	3%	0.001
CFNI	205	6%	0.0005

Therefore, the corrosion resistance of various steel–concrete systems can be ranked as CFN ≈ CFNI > CF > CC. Then, these results were confirmed using Bode modulus plots given in Fig. 8b. These plots show the variations in the impedance with a change in frequency for all the four concrete systems. Similar EIS spectra have been reported for OPC concrete specimens and fly ash modified

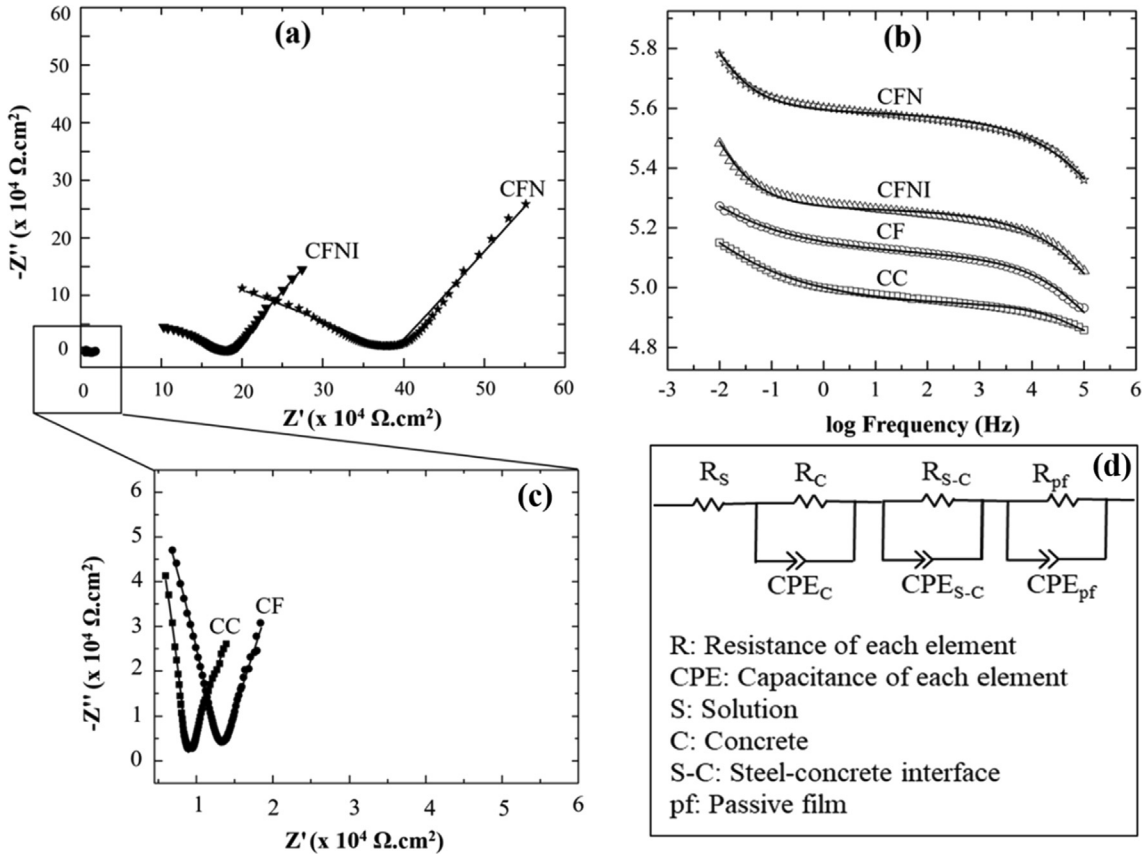

Fig. 8. (a) Nyquist plots (b) bode modulus plots obtained from the EIS measurements (c) magnified view of the boxed region of Fig. 8a and (d) equivalent circuit used for fitting the electrochemical impedance data [71].

specimens [17,83]. A commonly accepted model for the steel/concrete interface is a passive thin film consisting of layers of iron oxides and hydroxides and also an interfacial film attached to the concrete matrix [53]. The main process involved in the impedance measurements is the charge transfer taking place at the interface of the substrate/electrolyte. It is related to the passive film formed on the surface of the metal under the exposed environment [84]. In the case of steel reinforcements embedded inside concrete structures, the highly alkaline environment provided by the concrete helps in the formation of the passive film on the rebar surface, which protects it from the initiation of corrosion. Generally, a system with good corrosion resistance will show high resistance values and lower capacitance values [54].

Fig. 9 shows the macrocell corrosion current determined from macrocell corrosion measurements. After three cycles of exposure, the half-cell potential of the CC concrete system started to shoot up and reached up to −300 $mV_{Ag/AgCl}$ indicating the severe corrosion of the anode. However, all the rebars embedded in modified concrete systems retained the passive condition-indicating the effect of mineral additions and supplementary cementitious materials in improving the corrosion resistance of the reinforcement. Fig. 9 also shows that the macrocell current was high for CC specimens at the end of six exposure cycles; whereas, CFN and CFNI specimens showed negligible macrocell corrosion current up to 120 days (five cycles) of exposure. After five cycles of exposure, all the concrete systems showed an increase in macrocell current. Further, on completion of six cycles of exposure, the rate of corrosion for CC and CF concrete specimens was found to be more than two times that of CFN and CFNI concrete specimens indicating the improved corrosion resistance of the embedded rebars in CFN and CFNI concrete.

3.4. Measurement of pH and conductivity of the aqueous concrete powder solution

The level of alkalinity of concrete indicated by its pH value influences the corrosion of reinforced concrete structures [85]. The pH of OPC concrete usually lies between 12.5 and 13, but chloride ingress into concrete results in a pH reduction due to the formation of hydrochloric acid [86]. Table 7 shows that the pH was reduced by about 5–10% of the initial pH on all the specimens after exposure. When the pH of concrete decreases, corrosion in reinforced concrete can occur at lower threshold chloride concentrations. A drop in the pH of concrete to values less than 11 near the vicinity of the rebars, result in the initiation of an active corrosion process in the presence of even nearly zero ppm of chloride ions [85].

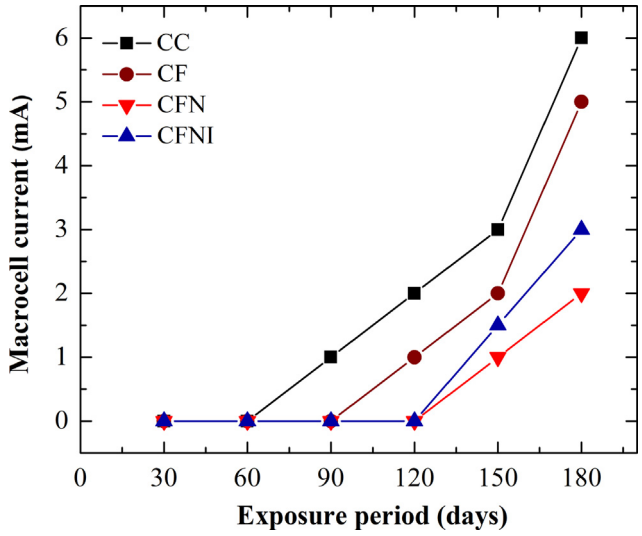

Fig. 9. Variations in ASTM G109 macrocell current of the TMT rebars inside various concrete systems (CC, CF, CFN and CFNI) with exposure time.

The addition of mineral admixtures resulted in the absorption of calcium hydroxide (CH) due to the pozzolanic reaction. Cement hydration leads to the formation of CH in the concrete system which improves the alkalinity of concrete [39]. Further, the amount of cement in concrete is reduced when mineral admixtures are added as partial cement replacement materials. This results in a reduction in the amount of CH produced by the cement hydration process. The reduction in pH leads to the destruction of the passive layer over the metal surface which in turn increases the rate of corrosion. However, all the specimens had pH more than 11, and hence steel bars were passivated. The least reduction of pH in CFN and CFNI contributes to the improved corrosion resistance of the reinforcements.

It could be seen from Table 7 that the free chloride contents in CC specimens are the highest (7.751 g/L) and the least in CFNI specimens (0.984 g/L). The chloride contents in CFN and CF concrete systems are 1.370 g/L and 3.799 g/L, respectively. This indicates that CFNI has the highest chloride binding capacity and most of the chlorides are in bound form rather than in free form. Therefore, the presence of free chlorides adversely affects the reinforcements in the concrete structures. Many researchers reported that the addition of the supplementary cementitious materials results in a significantly higher reduction in the permeability of concrete due to their pozzolanic reaction which leads to low ingress of deleterious chloride ions [87,88]. On addition to cement, $CaCO_3$ nanoparticles react with the aluminium oxides present in cement and form carboaluminate hydrates, besides accelerating C_3S and C_3A hydration [89]. The increased C_3A content reduces the free chloride concentration in the concrete pore solution and forms a dense structure where the ionic transport is minimal as the diffusion of chloride ions depends on the permeability [90]. Thus, in CFN and CFNI concretes the chlorides are present in the bound form of Friedel's salt.

Femenias et al. [91] developed a novel methodology to simultaneously monitor the pH of the concrete pore solution and free chloride concentration and reported that both these parameters are highly relevant to the corrosion control of the reinforcing steel. It is known that the risk of corrosion increases with the increased ratio of chloride to hydroxyl ion concentrations (Cl^-/OH^-). Thus, it is highly important to obtain data on chloride concentration and pH when steel rebars are embedded in concrete. In this study, the CFNI concrete specimens showed a comparatively lower reduction in pH values (5.55%) and the low free chloride concentration (0.984 g/L).

Table 7 shows that the conductivity value is the highest for CC specimens (3140 μs/cm) and the lowest for CFNI specimens (1364 μs/cm). This indicates the presence of more free chloride ions in CC as compared to CFNI. Higher conductivity leads to a higher cathodic reaction rate that can result in accelerated corrosion. The low conductivity of CFNI specimens is found to be due to the reduced permeability in these specimens owing to the low w/c ratio and the refined pore structure [39].

3.5. Morphological and chemical characterization of the corroded concrete-steel interface

3.5.1. FESEM analysis and elemental mapping

Fig. 10 shows the FESEM images indicating the surface topography of the powders extracted from the corroded concrete-steel interface of all four types of concrete systems after 180 days of exposure in a 3.5% NaCl solution. The surface of the CC concrete

Table 7
pH, conductivity and free chloride contents for all concrete systems after exposure in 3.5% NaCl solution for 180 days.

Type of specimen	pH		reduction in pH (%)	Conductivity (μs/cm)	Free chloride content (g/L)
	Initial	Final			
CC	12.9	12.2	5.42	3140	7.751
CF	12.1	11.1	8.26	2260	3.799
CFN	12.7	11.8	7.08	1640	1.370
CFNI	12.6	11.9	5.55	1364	0.984

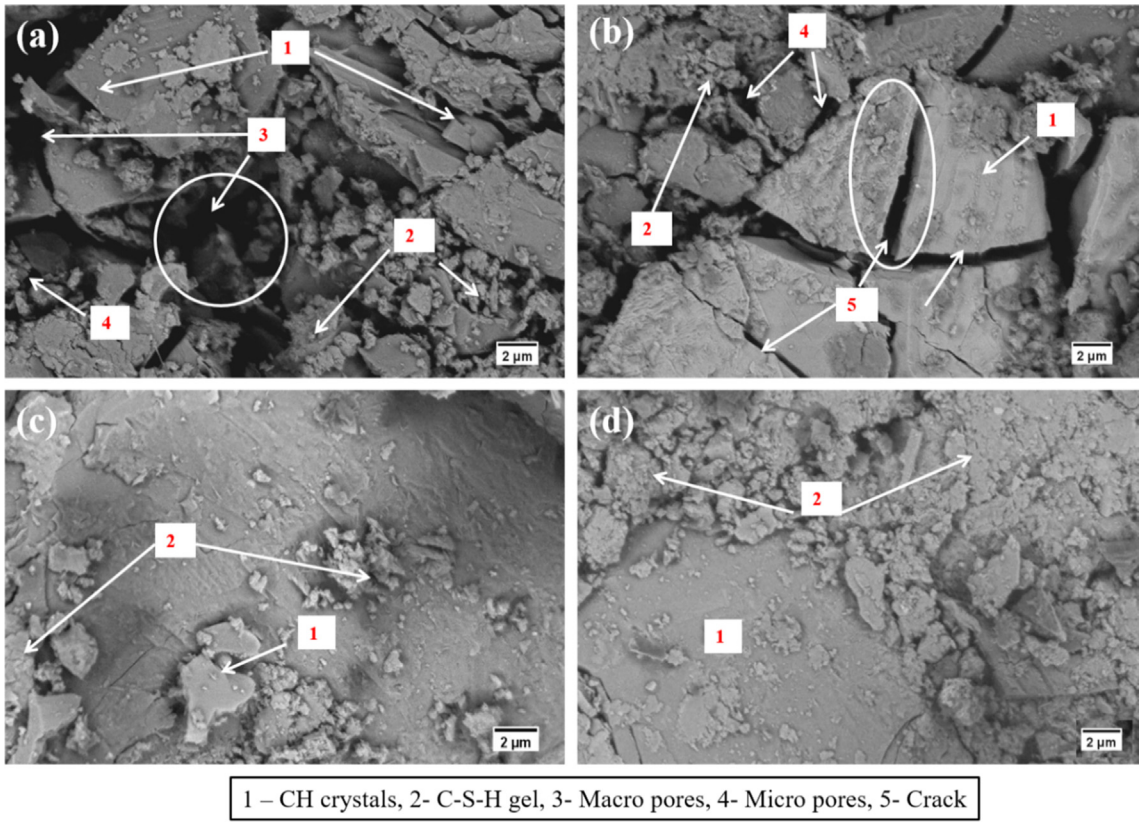

Fig. 10. FESEM topographies of the powders extracted from the concrete- steel interface for all specimens after 180 days of exposure in 3.5% NaCl solution (a) CC (b) CF (c) CFN and (d) CFNI.

showed the presence of more micropores and macropores than that on other concrete specimens, indicating severe corrosion (Fig. 10a). Calcium hydroxide (CH) crystals produced from the hydration of cement can also be seen in the Figure. The calcium silicate hydrate (CSH) gel formation, resulting from the hydration in concrete, is less on the surface of the CC concrete system. The presence of pores and cracks are also visible over the surface of fly ash modified CF concrete specimens (Fig. 10b). The surface of the CFN specimen showed more CSH gel and CH content as a result of the added nanomodifiers. No visible cracks or pores are observed on the surface of CFN specimens (Fig. 10c). CFNI specimens showed the presence of enhanced CH content and uniformly packed CSH gel resulting from the hydration process in concrete due to the inhibitor (Fig. 10d).

The elemental analysis of the powder samples extracted from the corroded concrete-steel interface is shown in Fig. 11. It can be observed that the Fe and O contents were more on the CC and CF concrete systems indicating more corrosion in these specimens. In all the concrete systems, except the CF system, Ca and Si contents were predominant due to the enhanced hydration process. However, the CF specimen was depleted of Ca (Fig. 11f) which is reported to be one of the disadvantages of using fly ash as a replacement material [27]. The Fe and O content in both CFN and CFNI specimens were found to be less as compared to CC and CF specimens, indicating the improvement in the corrosion resistance in these specimens. The elemental mapping of the corroded extracts confirmed the enhancement in the corrosion properties due to the addition of nanomodifiers and inhibitor.

3.5.2. XRD analysis

Fig. 12 shows the X-ray diffraction spectra of the powder samples extracted from the corroded concrete-steel interface of all the four concrete systems after 180 days of exposure in a 3.5% NaCl solution. The peaks corresponding to the hydration products in concrete, such as quartz and CSH were present in the spectra of all the concretes. Among all the systems, CFNI specimens showed the highest intensity peaks of both quartz and CSH, indicating the superior properties of this composition. A high amount of SiO_2 accelerates the secondary hydration reaction leading to the formation of more CSH gel, which reduces the permeability and porosity of concrete. This, in turn, reduces the ingress and diffusion of the chloride ions into the specimens through the pores and thus reduces the corrosion rate of the embedded steel reinforcement [16].

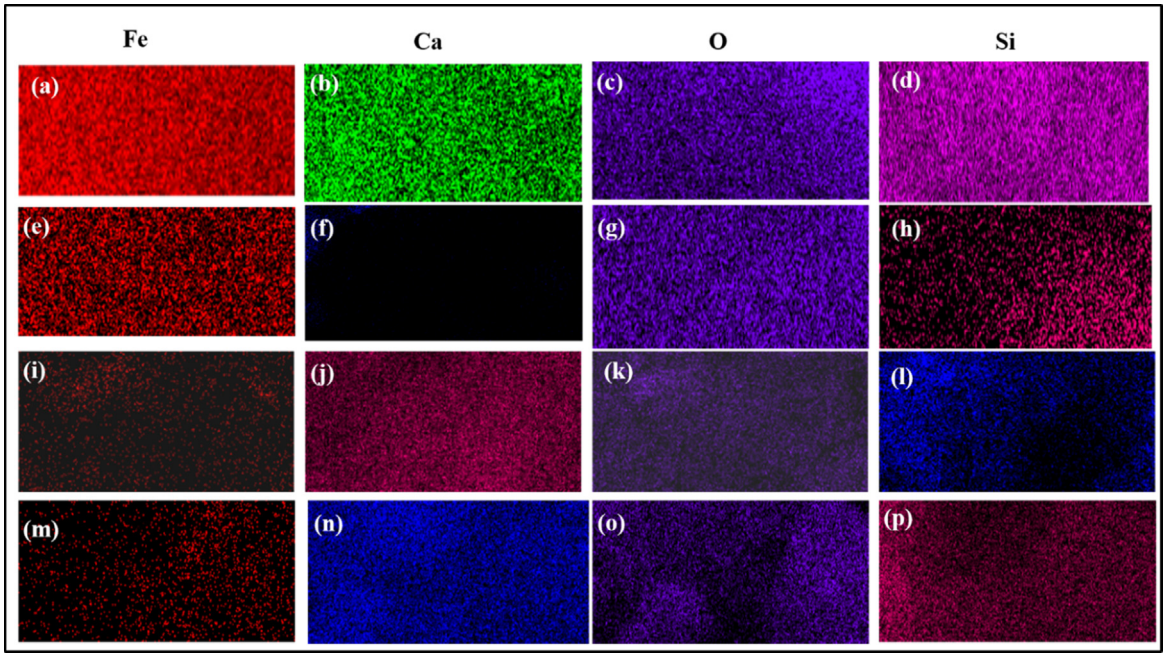

Fig. 11. Elemental mapping of the concrete-steel interface for all specimens after 180 days of exposure in 3.5% NaCl solution (a-d) CC (e-h) CF (i-l) CFN and (m-p) CFNI. The images are taken on a scale of 2.5 μm.

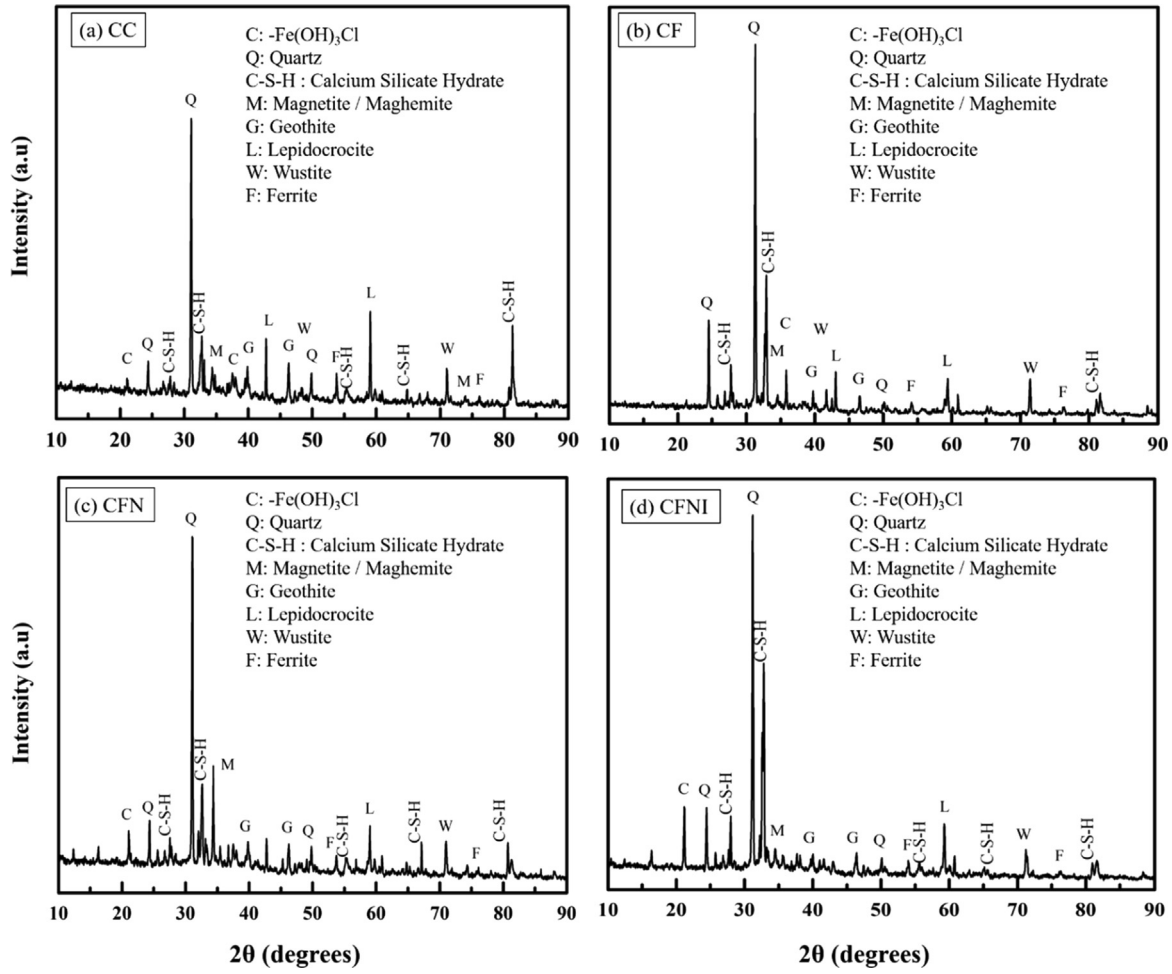

Fig. 12. X-ray Diffraction spectra of the concrete specimens surrounding the corroded rebar after 180 days of exposure in 3.5% NaCl solution (a) CC (b) CF (c) CFN and (d) CFNI.

The spectra of all the systems showed some peaks of ferrite resulting from the mild steel rebar. The corrosion products like lepidocrocite, goethite (α –FeOOH), wustite and magnetite were identified in the spectra of all the concrete systems. It is reported that both lepidocrocite and goethite produce the highest volume expansion ratio, which can result in cracking of the concrete specimens [92]. Further, a ferrous hydroxychloride phase ($Fe(OH)_3Cl$), which is an intermediate phase to akaganeite was also identified in all the spectra [93]. Among all the specimens, the intensities of the peaks corresponding to the corrosion products were the highest in CC specimens (Fig. 12a). CF specimens showed a reduction in the intensities and the number of peaks of corrosion products from what is observed for CC specimens. The least number of peaks with the lower intensities of corrosion products are observed in CFNI and CFN specimens.

3.5.3. Thermogravimetric analysis – chloride binding capacity and pH

Fig. 13 shows the results of the thermogravimetric analysis carried out on powder samples extracted from the near vicinity of the corroded concrete-steel interface after 180 days of exposure in the electrolyte. The DTG curves of the powdered samples are shown in Fig. 13a. Similar DTG curves were reported by Shi et al. [68], in which three endothermic peaks corresponding to mass losses are observed on heating from room temperature to 1200 °C, i.e., C-S-H (30–230 °C), CH (410–520 °C) and $CaCO_3$ (520–760 °C). The Friedel's salt profile and the endothermic peak corresponding to the formation of Friedel's salt [68] were compared with the DTG curve obtained in this study to confirm its presence. The shoulder representing the formation of Friedel's salt showed the maximum intensity for CFNI specimen and the lowest intensity for CC specimen. This indicates the presence of more bound chlorides in the CFNI concrete system. The peak corresponding to CH is seen predominant in all the concrete specimens, indicating high alkalinity. The formation of $CaCO_3$, corresponding to the the extent of carbonation process in the concrete specimens is also compared. It is observed that CF specimens showed the highest carbonation as reported in the previous study [39].

The amount of Friedel's salt in concrete gives an idea about the chloride binding capacity of concrete. Fig. 13b shows that the mass loss due to the formation of Friedel's salt is found to be the highest in CFNI specimens (2.38%), indicating the presence of a surplus amount of bound chloride with less amount of free chlorides. Friedel's salt formation is found to be the minimum (1.62%) in CC specimens. CF and CFN specimens showed a mass loss of 1.69 and 1.84%, respectively indicating their improved chloride binding capacity as compared to the control specimens. The thermogravimetric analysis was also used to estimate the portlandite content, which indicates the alkalinity of the concrete specimen after exposure in 3.5% NaCl solution and is shown in Fig. 13b. CC specimens showed the highest mass loss of 0.82% and CF specimens showed the least mass loss of 0.57%. The mass loss in CFN and CFNI specimens are 0.61 and 0.72%, respectively. These results show that the addition of fly ash has resulted in the consumption of $Ca(OH)_2$ in CF specimens.

The amount of Friedel's salt and portlandite estimated using the above method is described in section 3.7.3 and is shown in Fig. 13c. The Friedel's salt content was found to be the highest in CFNI specimens (12.36 wt%) and the lowest in CC specimens (8.41 wt%). Frie-

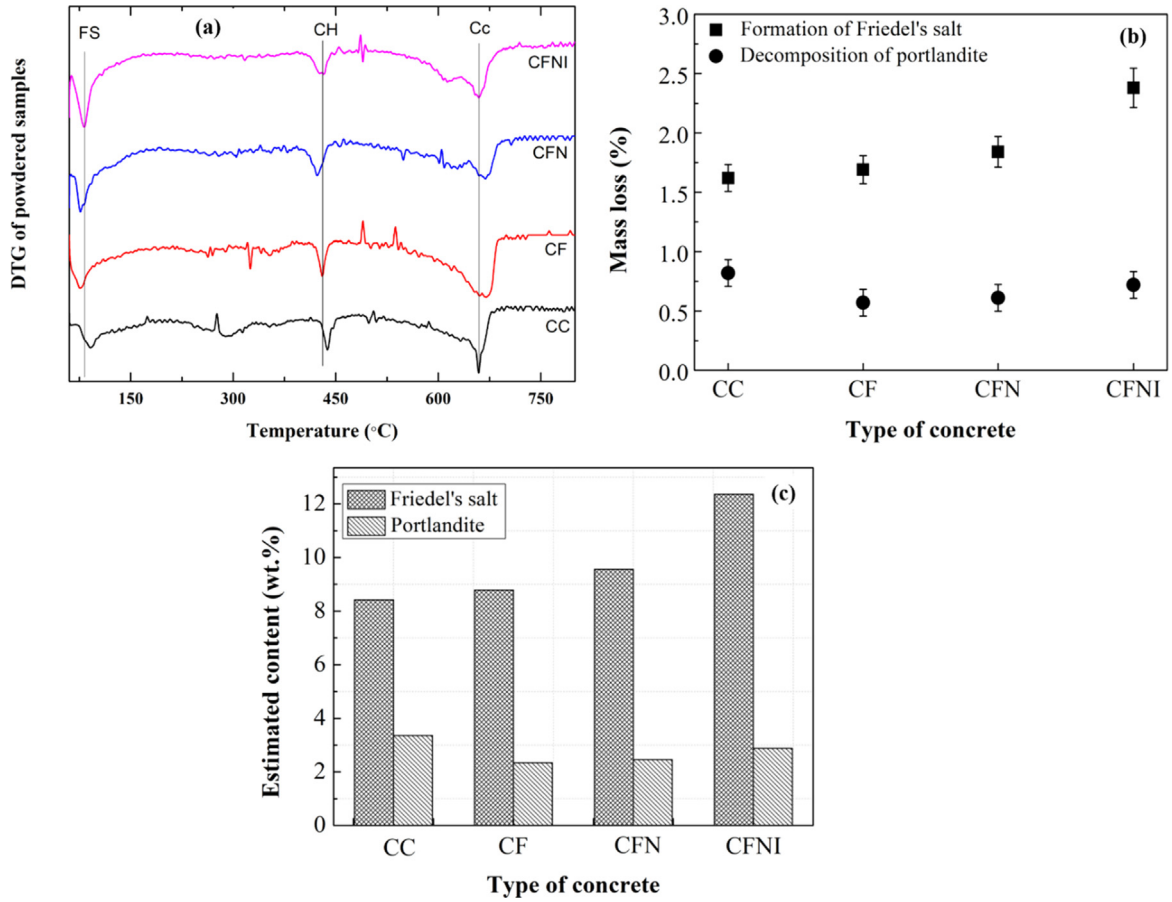

Fig. 13. (a) DTG curves of the powdered samples from the concrete-steel interface (b) mass loss due to the formation of Friedel's salt and decomposition of portlandite (c) estimated amount of Friedel's salt and portlandite from TGA analysis of the concrete-steel interface after 180 days of exposure in 3.5% NaCl solution.

del's salt content of CF and CFN specimens are 8.78 and 9.56 wt%, respectively. The thermogravimetric analysis of the corroded concrete-steel interface indicated the presence of more Friedel's salt, due to the presence of more bound chlorides in CFNI specimens. The presence of free chlorides is detrimental to the reinforcements inside the concrete structures. If chloride ions are present in the bound form, the process of corrosion initiation will be delayed. These results are consistent with the observations of free chloride contents in Table 7.

The estimated portlandite content is shown in Fig. 13c. CC specimens showed the highest $Ca(OH)_2$ content of 3.36 wt%, owing to the more amount of cement per unit volume and CF specimens showed the lowest $Ca(OH)_2$ content of 2.33 wt%. The addition of nanoparticles and inhibitor to fly ash admixed concrete improved the $Ca(OH)_2$ content in CFN (2.46 wt%) and CFNI (2.88 wt%) specimens, which resulted in high pH value in these specimens as compared to CF specimens. This is in good agreement with the pH measurements. Thus, thermogravimetric analysis helped to establish the increased corrosion resistance of CFNI concrete in a highly chloride environment.

3.5.4. FTIR spectroscopic measurements

FTIR spectra of the powder samples extracted from the corroded concrete-steel interface of all the four concrete systems are shown in Fig. 14. The peaks corresponding to the main corrosion product of mild steel (lepidocrocite), was found in the spectra of all four samples at 1035 cm^{-1} [94]. However, in the case of the CC powder sample (Fig. 14a), an additional peak at 874 cm^{-1} corresponding to lepidocrocite was also observed. The peak at 774 cm^{-1} corresponding to goethite, a transformed form of lepidocrocite was also observed in the spectra of all the powder samples [95]. The intensities of the peaks corresponding to both lepidocrocite and goethite were the maximum in the case of CC specimens, indicating severe corrosion in these specimens. Both CFN and CFNI specimens showed less intense peaks of lepidocrocite and goethite, due to the improved corrosion resistance.

The peak at 1436 cm^{-1} corresponds to the asymmetric stretching vibrations of carbonate ions, which was present in all the powder samples, indicating the carbonation in these specimens [96]. A high intense peak at 1634 cm^{-1} in CC specimens is attributed to the water molecules in the powder samples [97]. The narrow absorption band at 3642 cm^{-1} corresponds to the stretching mode of O–H from $Ca(OH)_2$ in all the powder samples [98]. Both CC and CFNI specimens showed comparatively higher intensity peaks of $(OH)^-$, which is also reflected in the pH values in these specimens. Thus, the high pH and fewer corrosion products in CFNI specimens confirm its superior corrosion resistance.

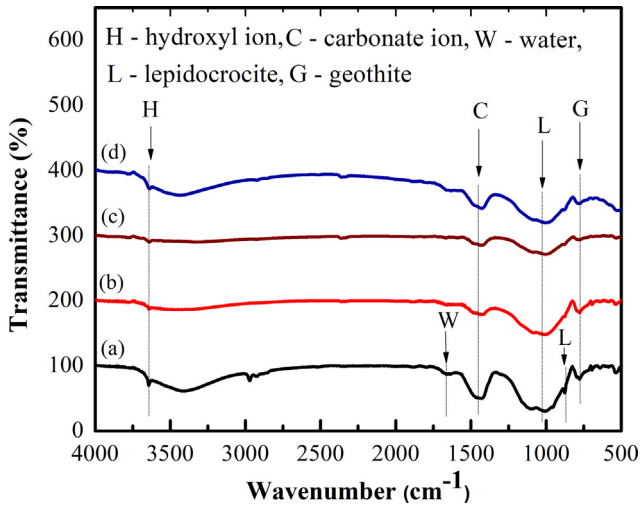

Fig. 14. FTIR spectra of the concrete-steel interface after 180 days of exposure in 3.5% NaCl solution (a) CC (b) CF (C) CFN and (d) CFNI.

3.6. Estimation of service life

Fig. 15 shows the Cumulative Distribution Function (CDF) of t_i for the girder element for all the four concrete mixes. A 50% probability of initiation of corrosion was considered to be failure criteria which decide the end of service life. The t_i for CC and CF concrete compositions was found to 25 and 35 years, respectively. However, the bridge girder with CFN and CFNI concrete compositions were found to have a service life of approximately 75 and 150 years, respectively, which is about three and six times longer than that of CC. Considering the design life, CFNI type of concrete compositions can meet the requirement for the long service life of marine infrastructure. This can be attributed to the closely packed microstructure and reduced apparent diffusion coefficient of CFNI concrete. This suggests that ternary blends can enhance the service life of RC structures significantly.

Harilal et al. [39] have previously reported that the incorporation of fly ash, nanoparticles and sodium nitrite based corrosion inhibitor into conventional concrete can greatly enhance the chloride ion penetration resistance of concrete. This was evident from the low RCPT values, improved time to cracking and the reduced maximum anodic current seen in this concrete composition under accelerated testing conditions. In the present study, even though the addition of inhibitor improved the corrosion resistance by many folds, the electrochemical measurements on the inhibitor admixed concrete (CFNI) showed inferior properties than the nanoparticles admixed concrete (CFN). However, life prediction and other characterization data established the overall advantages of CFNI concrete composition. OCP monitoring and LPR techniques are considered as natural electrochemical experiments, whereas the accelerated corrosion testing (ACT) method is used frequently to reduce the time taken for obtaining a critical level of chlorides on the surface of the reinforcement. In ACT test, CFNI showed the highest corrosion resistance due to the combined action of nps and inhibitor [39].

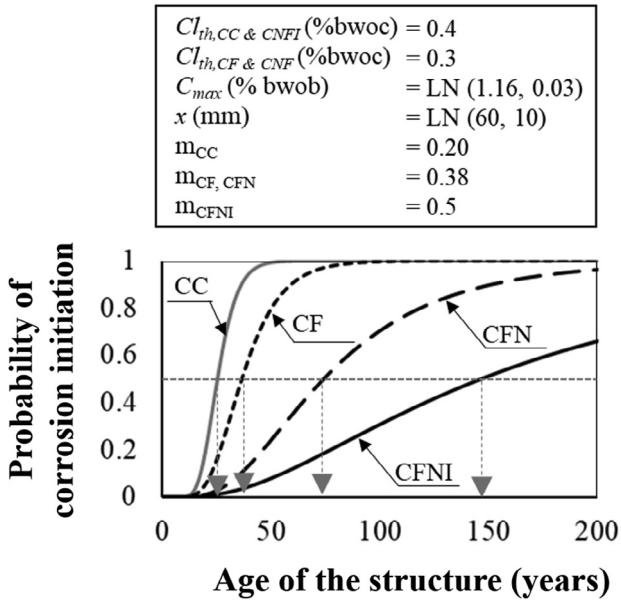

Fig. 15. Cumulative distribution function of time to corrosion initiation vs age of concrete (years) for different concrete specimens.

It is possible that the addition of inhibitor and nanoparticles together may take comparatively longer exposure periods to realize their combined effect from electrochemical measurements. A combination of fly ash and inhibitor alone is being attempted to establish the individual effect of inhibitor in fly ash modified concrete.

4. Conclusions

The combined effect of fly ash, nanoparticles, and inhibitor in enhancing the corrosion resistance of reinforcements embedded inside a newly developed M45 grade concrete composition (CFNI) was investigated using chloride diffusion coefficients and electrochemical measurements. The following conclusions were drawn from the present study:

1. The chloride concentrations on the surface of CFNI and CFN concrete specimens were significantly higher than those on CC and CF specimens, indicating an improved chloride binding capacity.
2. The value of D_{cl} for CFNI concrete was found to be one order less in magnitude than other concrete specimens, indicating the enhanced resistance against chloride attack.
3. The corrosion current density values of rebars embedded in CFNI and CFN test specimens showed values corresponding to the low severity region, indicating the higher resistance to corrosion activities.
4. The average corrosion rates for all the modified concrete systems determined using the LPR and gravimetric measurements show that that the use of fly ash, nanomaterials, inhibitors, or a combination of them can enhance the corrosion resistance of RC systems.
5. From the EIS measurement results, the resistance of passive film of steel embedded in CFNI concrete is higher than the resistance of passive film of steel embedded in all other concrete systems. The conductivity measurements and free chloride contents also corroborated the EIS studies.
6. The FESEM images showed no micro cracks or pores over the surface of CFNI and CFN specimens. The Fe and O content determined through elemental mapping in both CFN and CFNI specimens were also found to be lower, indicating an improved corrosion resistance in these specimens.
7. The thermogravimetric analysis of the corroded concrete-steel interface indicated the presence of more Friedel's salt, which results from the presence of more bound chlorides in CFNI specimens.
8. The probabilistic service life of the steel in concrete systems, estimated using the measured chloride diffusion coefficients, showed that the time to initiation of corrosion in CFNI specimens is six times higher than the control mix with OPC.

These results suggest that the CFNI type of concrete gives significantly enhanced service life in aggressive marine environments.

CRediT authorship contribution statement

Manu Harilal: Conceptualization, Methodology, Software, Visualization, Writing - original draft. **Deepak K. Kamde:** Software, Visualization, Methodology, Investigation. **Sudha Uthaman:** Investigation. **R.P. George:** Supervision, Writing - review & editing. **Radhakrishna G. Pillai:** Supervision, Writing - review & editing. **John Philip:** Supervision, Writing - review & editing. **Shaju.K. Albert:** Supervision, Writing - review & editing.

Declaration of Competing Interest

The authors declare that they have no known competing financial interests or personal relationships that could have appeared to influence the work reported in this paper.

Acknowledgements

The fellowship provided by DAE, Govt. of India for carrying out this research is greatly acknowledged. The authors sincerely acknowledge the Director, IGCAR and Dr. S. Raju, AD, MCG for their support. Mr. Rathish.V. R. and Dr. M.S. Haji Sheik Mohammed are acknowledged for their extended help in providing laboratory facility for casting the specimens and Ms. Geetisubhra Jena, MMG, IGCAR for the useful technical discussions.

References

[1] K. Tamanna, S.N. Raman, M. Jamil, R. Hamid, Utilization of wood waste ash in construction technology: a review, Constr. Build. Mater. 237 (2020) 117654, https://doi.org/10.1016/j.conbuildmat.2019.117654.
[2] F.-C. Lo, S.-L. Lo, M.-G. Lee, Effect of partially replacing ordinary Portland cement with municipal solid waste incinerator ashes and rice husk ashes on pervious concrete quality, Environ. Sci. Pollut. Res. 27 (19) (2020) 23742–23760, https://doi.org/10.1007/s11356-020-08796-z.
[3] E. Benhelal, A. Rafiei, E. Shamsaei, Green cement production: potentials and achievements, IJCEA (2012) 407–409, https://doi.org/10.7763/IJCEA.2012.V3.229.
[4] X. Chen, H. Wang, H. Najm, G. Venkiteela, J. Hencken, Evaluating engineering properties and environmental impact of pervious concrete with fly ash and slag, J. Cleaner Prod. 237 (2019) 117714, https://doi.org/10.1016/j.jclepro.2019.117714.
[5] M. Manera, Ø. Vennesland, L. Bertolini, Chloride threshold for rebar corrosion in concrete with addition of silica fume, Corros. Sci. 50 (2) (2008) 554–560, https://doi.org/10.1016/j.corsci.2007.07.007.
[6] M. Reiner, S.A. Durham, K.L. Rens, Development and analysis of high-performance green concrete in the urban infrastructure, Int. J. Sustainable Eng. 3 (3) (2010) 198–210, https://doi.org/10.1080/19397031003746662.
[7] I. Papanikolaou, N. Arena, A. Al-Tabbaa, Graphene nanoplatelet reinforced concrete for self-sensing structures – a lifecycle assessment perspective, J. Cleaner Prod. 240 (2019) 118202, https://doi.org/10.1016/j.jclepro.2019.118202.
[8] G. Koch, J.V.N. Thompson, O. Moghissi, M. Gould, J. Payer, International measures of prevention, application, and economics of corrosion technologies study, NACE International (2016) 1–30. http://impact.nace.org/documents/Nace-International-Report.pdf.
[9] M. Jin, S. Gao, L. Jiang, H. Chu, M. Lu, F.F. Zhi, Degradation of concrete with addition of mineral admixture due to free chloride ion penetration under the effect of carbonation, Corros. Sci. 138 (2018) 42–53, https://doi.org/10.1016/j.corsci.2018.04.004.
[10] J. Kline, B. Pesic, K. Raja, I. Ehrsam, Corrosion studies of rebar in contact with saturated solution produced by leaching of Portland Type-II cement: examining the effects of chloride, carbonation and an amorphous silica additive, Corros. Eng., Sci. Technol. 53 (6) (2018) 431–443, https://doi.org/10.1080/1478422X.2018.1496219.
[11] R.B. Polder, W.H.A. Peelen, W.M.G. Courage, Non-traditional assessment and maintenance methods for aging concrete structures – technical and non-technical issues: non-traditional assessment and maintenance methods, Mater. Corros. 63 (12) (2012) 1147–1153, https://doi.org/10.1002/maco.201206725.
[12] D. Joseline, D.K. Kamde, S. Rengaraju, R.G. Pillai, Residual Service Life Estimation and its Importance for Pretensioned Concrete (PTC) Bridges in Coastal Cities, Sixth International Conference on Durability of Concrete Structures. United Kingdom (2019) 800–806.
[13] D.K. Kamde, R.G. Pillai, Effect of surface preparation on corrosion of steel rebars coated with cement-polymer-composites (CPC) and embedded in concrete, Constr. Build. Mater. 237 (2020) 117616, https://doi.org/10.1016/j.conbuildmat.2019.117616.
[14] J. Karuppanasamy, R.G. Pillai, A short-term test method to determine the chloride threshold of steel–cementitious systems with corrosion inhibiting admixtures, Mater. Struct. 50 (4) (2017), https://doi.org/10.1617/s11527-017-1071-1.
[15] Y. Zhao, J. Dong, Y. Wu, H. Wang, X. Li, Q. Xu, Steel corrosion and corrosion-induced cracking in recycled aggregate concrete, Corros. Sci. 85 (2014) 241–250, https://doi.org/10.1016/j.corsci.2014.04.028.
[16] K. De Weerdt, B. Lothenbach, M.R. Geiker, Comparing chloride ingress from seawater and NaCl solution in Portland cement mortar, Cem. Concr. Res. 115 (2019) 80–89, https://doi.org/10.1016/j.cemconres.2018.09.014.
[17] S.-J. Kwon, H.-S. Lee, S. Karthick, V. Saraswathy, H.-M. Yang, Long-term corrosion performance of blended cement concrete in the marine

environment – a real-time study, Constr. Build. Mater. 154 (2017) 349–360, https://doi.org/10.1016/j.conbuildmat.2017.07.237.
[18] S.P. Karthick, S. Muralidharan, V. Saraswathy, S.-J. Kwon, Effect of different alkali salt additions on concrete durability property, J. Struct. Integrity Maint. 1 (1) (2016) 35–42, https://doi.org/10.1080/24705314.2016.1153338.
[19] K. Tuutti, Corrosion of steel in concrete, Cement-och betonginst, 1982
[20] G.K. Glass, N.R. Buenfeld, The influence of chloride binding on the chloride induced corrosion risk in reinforced concrete, Corros. Sci. 42 (2) (2000) 329–344, https://doi.org/10.1016/S0010-938X(99)00083-9.
[21] S.-H. Han, Influence of diffusion coefficient on chloride ion penetration of concrete structure, Constr. Build. Mater. 21 (2) (2007) 370–378, https://doi.org/10.1016/j.conbuildmat.2005.08.011.
[22] Q. Yuan, C. Shi, G. De Schutter, K. Audenaert, D. Deng, Chloride binding of cement-based materials subjected to external chloride environment – a review, Constr. Build. Mater. 23 (1) (2009) 1–13, https://doi.org/10.1016/j.conbuildmat.2008.02.004.
[23] C. Alonso, M. Castellote, C. Andrade, Chloride threshold dependence of pitting potential of reinforcements, Electrochim. Acta 47 (21) (2002) 3469–3481, https://doi.org/10.1016/S0013-4686(02)00283-9.
[24] T. Van Gerven, G. Cornelis, E. Vandoren, C. Vandecasteele, A.C. Garrabrants, F. Sanchez, D.S. Kosson, Effects of progressive carbonation on heavy metal leaching from cement-bound waste, AIChE J. 52 (2) (2006) 826–837, https://doi.org/10.1002/aic.10662.
[25] T.-H. Ha, S. Muralidharan, J.-H. Bae, Y.-C. Ha, H.-G. Lee, K.-W. Park, D.-K. Kim, Accelerated short-term techniques to evaluate the corrosion performance of steel in fly ash blended concrete, Build. Environ. 42 (1) (2007) 78–85, https://doi.org/10.1016/j.buildenv.2005.08.019.
[26] T.R. Naik, S.S. Singh, M.M. Hossain, Permeability of concrete containing large amounts of fly ash, Cem. Concr. Res. 24 (5) (1994) 913–922, https://doi.org/10.1016/0008-8846(94)90011-6.
[27] V. Vishwakarma, R.P. George, D. Ramachandran, B. Anandkumar, U.K. Mudali, Studies of detailed Biofilm characterization on fly ash concrete in comparison with normal and superplasticizer concrete in seawater environments, Environ. Technol. 35 (1) (2014) 42–51, https://doi.org/10.1080/09593330.2013.808249.
[28] F. Pacheco-Torgal, S. Jalali, Nanotechnology: advantages and drawbacks in the field of construction and building materials, Constr. Build. Mater. 25 (2) (2011) 582–590, https://doi.org/10.1016/j.conbuildmat.2010.07.009.
[29] S. Uthaman, V. Vishwakarma, R.P. George, D. Ramachandran, K. Kumari, R. Preetha, M. Premila, R. Rajaraman, U.K. Mudali, G. Amarendra, Enhancement of strength and durability of fly ash concrete in seawater environments: synergistic effect of nanoparticles, Constr. Build. Mater. 187 (2018) 448–459, https://doi.org/10.1016/j.conbuildmat.2018.07.214.
[30] Koleva, An Innovative Approach to Control Steel Reinforcement Corrosion by Self-Healing, Materials, 11 (2018) 309. https://doi.org/10.3390/ma11020309
[31] T.H. Nguyen, T.A. Nguyen, Protection of steel rebar in salt-contaminated cement mortar using epoxy nanocomposite coatings, Int. J. Electrochem. 2018 (2018) 1–10, https://doi.org/10.1155/2018/8386426.
[32] M.S. Al-Otaibi, A.M. Al-Mayouf, M. Khan, A.A. Mousa, S.A. Al-Mazroa, H.Z. Alkhathlan, Corrosion inhibitory action of some plant extracts on the corrosion of mild steel in acidic media, Arabian J. Chem. 7 (3) (2014) 340–346, https://doi.org/10.1016/j.arabjc.2012.01.015.
[33] W. Morris, M. Vazquez, Corrosion of reinforced concrete exposed to marine environment, Corros. Rev. 20 (2002) 469-508. https://doi.org/10.1515/CORRREV.2002.20.6.469
[34] K.A.A. Al-Sodani, O.S.B. Al-Amoudi, M. Maslehuddin, M. Shameem, Efficiency of corrosion inhibitors in mitigating corrosion of steel under elevated temperature and chloride concentration, Constr. Build. Mater. 163 (2018) 97–112, https://doi.org/10.1016/j.conbuildmat.2017.12.097.
[35] A. Cook, S. Ranke, Chloride corrosion of steel in concrete, ASTM-STP 629 (1977) 51–60.
[36] R. Craig, L. Wood, Effectiveness of corrosion inhibitors and their influence on the physical properties of Portland cement mortars, Highway Res. Rec. (1970).
[37] R.A.D. Treadaway K. W. J., Highways and Public Works, 1968
[38] V. Tamizhselvi, K. Samuel, Electrochemical investigations to evaluate the performance of inhibitors to control rebar corrosion, Indian Concr. Inst. J. 8 (2007) 7–13.
[39] Manu Harilal, V.R. Rathish, B. Anandkumar, R.P. George, M.S. Haji Sheikh Mohammed, John Philip, G. Amarendra, High performance green concrete (HPGC) with improved strength and chloride ion penetration resistance by synergistic action of fly ash, nanoparticles and corrosion inhibitor, Constr. Build. Mater. 198 (2019) 299–312, https://doi.org/10.1016/j.conbuildmat.2018.11.266.
[40] Manu Harilal, Sudha Uthaman, B. Anandkumar, B.B. Lahiri, R.P. George, John Philip, G. Amarendra, Fungal resistance of nanomodifiers and corrosion inhibitor amended fly ash concrete, Int. Biodeterior. Biodegrad. 143 (2019) 104725, https://doi.org/10.1016/j.ibiod.2019.104725.
[41] M. Harilal, S. Uthaman, R. George, B. Anandkumar, C. Thinaharan, J. Philip, U.J. E.P. Kamachi Mudali, S. Energy, Enhanced anti-microbial activity in green concrete specimens containing fly ash, nanophase modifiers, and corrosion inhibitor, 38(4) (2019) 13102. https://doi.org/10.1002/ep.13102
[42] ASTM C494/C494M-19, Standard Specification for Chemical Admixtures for Concrete, Annual Book of ASTM Standards, ASTM International, West Conshohocken, PA, 2004.
[43] K.Y. Ann, J.H. Ahn, J.S. Ryou, The importance of chloride content at the concrete surface in assessing the time to corrosion of steel in concrete structures, Constr. Build. Mater. 23 (1) (2009) 239–245, https://doi.org/10.1016/j.conbuildmat.2007.12.014.
[44] Mahmoud Shakouri, David Trejo, A time-variant model of surface chloride build-up for improved service life predictions, Cem. Concr. Compos. 84 (2017) 99–110, https://doi.org/10.1016/j.cemconcomp.2017.08.008.
[45] Ha-Won Song, Chang-Hong Lee, Ki Yong Ann, Factors influencing chloride transport in concrete structures exposed to marine environments, Cem. Concr. Compos. 30 (2) (2008) 113–121, https://doi.org/10.1016/j.cemconcomp.2007.09.005.
[46] Yuvaraj Dhandapani, T. Sakthivel, Manu Santhanam, Ravindra Gettu, Radhakrishna G. Pillai, Mechanical properties and durability performance of concretes with Limestone Calcined Clay Cement (LC3), Cem. Concr. Res. 107 (2018) 136–151, https://doi.org/10.1016/j.cemconres.2018.02.005.
[47] ASTM C1556–11a, Standard Test Method for Determining the Apparent Chloride Diffusion Coefficient of Cementitious Mixtures by Bulk Diffusion, Annual Book of ASTM Standards, ASTM International, West Conshohocken, PA, 2015.
[48] SHRP-S-330, Standard Test Method for Chloride Content in Concrete Using the Specific Ion Probe (1993) 1–118.
[49] E.C. Bentz, Probabilistic modeling of service life for structures subjected to chlorides, ACI Mater. J. 100 (2003) 391–397.
[50] LIFE 365, Software V2.2, http://www.life-365.org/
[51] U. Raghu Babu, B. Kondraivendhan, Effect of IR Drop on Reinforced Concrete Corrosion Measurements, Materials Science and Engineering Conference Series, (2020), 012015. https://doi.org/10.1088/1757-899X/829/1/012015
[52] ASTM G59–97, Standard Test Method for Conducting Potentiodynamic Polarization ResistanceMeasurements, Annual Book of ASTM Standards, ASTM International, West Conshohocken, PA, 2014.
[53] Mohamed Ismail, Masayasu Ohtsu, Corrosion rate of ordinary and high-performance concrete subjected to chloride attack by AC impedance spectroscopy, Constr. Build. Mater. 20 (7) (2006) 458–469, https://doi.org/10.1016/j.conbuildmat.2005.01.062.
[54] Velu Saraswathy, Ha-Won Song, Electrochemical studies on the corrosion performance of steel embedded in activated fly ash blended concrete, Electrochim. Acta 51 (22) (2006) 4601–4611, https://doi.org/10.1016/j.electacta.2006.01.005.
[55] J. Blunt, G. Jen, C.P. Ostertag, Enhancing corrosion resistance of reinforced concrete structures with hybrid fiber reinforced concrete, Corros. Sci. 92 (2015) 182–191, https://doi.org/10.1016/j.corsci.2014.12.003.
[56] C. Andrade, J.A. González, Quantitative measurements of corrosion rate of reinforcing steels embedded in concrete using polarization resistance measurements, Mater. Corros. 29 (8) (1978) 515–519, https://doi.org/10.1002/maco.19780290804.
[57] J. Flis, S. Sabol, H.W. Pickering, A. Sehgal, K. Osseo-Asare, P.D. Cady, Electrochemical measurements on concrete bridges for evaluation of reinforcement corrosion rates, Corrosion 49 (7) (1993) 601–613, https://doi.org/10.5006/1.3316091.
[58] M.A. Pech-Canul, P. Castro, Corrosion measurements of steel reinforcement in concrete exposed to a tropical marine atmosphere, Cem. Concr. Res. 32 (3) (2002) 491–498, https://doi.org/10.1016/S0008-8846(01)00713-X.
[59] ASTM G1–90A, Standard Practice for Preparing, Cleaning, and Evaluating Corrosion Test Specimens, Annual Book of ASTM Standards, ASTM International, West Conshohocken, PA, 1999.
[60] V. Saraswathy, Ha-Won Song, Improving the durability of concrete by using inhibitors, Build. Environ. 42 (1) (2007) 464–472, https://doi.org/10.1016/j.buildenv.2005.08.003.
[61] ASTM G109-07A, Standard Test Method for Determining Effects of Chemical Admixtures on Corrosion of Embedded Steel Reinforcement in Concrete Exposed to Chloride Environments, Annual Book of ASTM Standards, ASTM International, West Conshohocken, PA, 2013.
[62] M.S. Haji Sheik Mohammed, R. Srinivasa Raghavan, G.M. Samuel Knight, V. Murugesan, Macrocell corrosion studies of coated rebars, Arab. J. Sci. Eng. 39 (5) (2014) 3535–3543, https://doi.org/10.1007/s13369-014-1006-x.
[63] V. Räsänen, V. Penttala, The pH measurement of concrete and smoothing mortar using a concrete powder suspension, Cem. Concr. Res. 34 (5) (2004) 813–820, https://doi.org/10.1016/j.cemconres.2003.09.017.
[64] Fouzia Shaheen, Bulu Pradhan, Influence of sulfate ion and associated cation type on steel reinforcement corrosion in concrete powder aqueous solution in the presence of chloride ions, Cem. Concr. Res. 91 (2017) 73–86, https://doi.org/10.1016/j.cemconres.2016.10.008.
[65] Jun Liu, Qiwen Qiu, Xiaochi Chen, Xiaodong Wang, Feng Xing, Ningxu Han, Yijian He, Degradation of fly ash concrete under the coupled effect of carbonation and chloride aerosol ingress, Corros. Sci. 112 (2016) 364–372, https://doi.org/10.1016/j.corsci.2016.08.004.
[66] L.K. Aggarwal, P.C. Thapliyal, S.R. Karade, Properties of polymer-modified mortars using epoxy and acrylic emulsions, Constr. Build. Mater. 21 (2) (2007) 379–383, https://doi.org/10.1016/j.conbuildmat.2005.08.007.
[67] Faiz U.A. Shaikh, Steve W.M. Supit, Mechanical and durability properties of high volume fly ash (HVFA) concrete containing calcium carbonate (CaCO3) nanoparticles, Constr. Build. Mater. 70 (2014) 309–321, https://doi.org/10.1016/j.conbuildmat.2014.07.099.
[68] Zhenguo Shi, Mette Rica Geiker, Klaartje De Weerdt, Tone Anita Østnor, Barbara Lothenbach, Frank Winnefeld, Jørgen Skibsted, Role of calcium on chloride binding in hydrated Portland cement–metakaolin–limestone blends, Cem. Concr. Res. 95 (2017) 205–216, https://doi.org/10.1016/j.cemconres.2017.02.003.

[69] Taehwan Kim, Jan Olek, Effects of sample preparation and interpretation of thermogravimetric curves on calcium hydroxide in hydrated pastes and mortars, Transp. Res. Rec. 2290 (1) (2012) 10–18, https://doi.org/10.3141/2290-02.
[70] Zhenguo Shi, Mette Rica Geiker, Barbara Lothenbach, Klaartje De Weerdt, Sergio Ferreiro Garzón, Kasper Enemark-Rasmussen, Jørgen Skibsted, Friedel's salt profiles from thermogravimetric analysis and thermodynamic modelling of Portland cement-based mortars exposed to sodium chloride solution, Cem. Concr. Compos. 78 (2017) 73–83, https://doi.org/10.1016/j.cemconcomp.2017.01.002.
[71] Sripriya Rengaraju, Lakshman Neelakantan, Radhakrishna G. Pillai, Investigation on the polarization resistance of steel embedded in highly resistive cementitious systems – An attempt and challenges, Electrochim. Acta 308 (2019) 131–141, https://doi.org/10.1016/j.electacta.2019.03.200.
[72] Radhakrishna G. Pillai, Ravindra Gettu, Manu Santhanam, Sripriya Rengaraju, Yuvaraj Dhandapani, Sundar Rathnarajan, Anusha S. Basavaraj, Service life and life cycle assessment of reinforced concrete systems with limestone calcined clay cement (LC3), Cem. Concr. Res. 118 (2019) 111–119, https://doi.org/10.1016/j.cemconres.2018.11.019.
[73] ASTM C876-09, Standard Test Method for Corrosion Potentials of Uncoated Reinforcing Steel in Concrete, Annual Book of ASTM Standards, ASTM International, West Conshohocken, PA (2009)
[74] R. Vedalakshmi, L. Balamurugan, V. Saraswathy, S. -H. Kim, K.Y. Ann, Reliability of Galvanostatic Pulse Technique in assessing the corrosion rate of rebar in concrete structures: Laboratory vs field studies, KSCE J. Civ. Eng. 14 (6) (2010) 867–877, https://doi.org/10.1007/s12205-010-1023-6.
[75] Xiaoyan Liu, Lei Chen, Aihua Liu, Xinrui Wang, Effect of nano-CaCO3 on properties of cement paste, Energy Procedia 16 (2012) 991–996, https://doi.org/10.1016/j.egypro.2012.01.158.
[76] M.M. Sadawy, E. Elsharkawy, Effect of nano-TiO2 addition on mechanical properties of concrete and corrosion behavior of reinforcement bars, IJERA 6 (2016) 61–65.
[77] Tuan Anh Nguyen, The Huyen Nguyen, Thi Lua Pham, Thi Mai Thanh Dinh, Hoang Thai, Xianming Shi, Application of nano-SiO 2 and nano-Fe 2 O 3 for protection of steel rebar in chloride contaminated concrete: epoxy nanocomposite coatings and nano-modified mortars, J. Nanosci. Nanotechnol. 17 (1) (2017) 427–436, https://doi.org/10.1166/jnn.2017.12396.
[78] B. Bavarian, L. Reiner, The Efficacy of using Migrating Corrosion Inhibitors (MCI 2020 & MCI 2020M) for Reinforced Concrete, 2004
[79] C. Andrade, M.C. Alonso, J.A. Gonzalez, An initial effort to use the corrosion rate measurements for estimating rebar durability, Corrosion rates of steel in concrete, ASTM International, 1990. https://doi.org/10.1520/STP25013S
[80] T. Frølund, F.M. Jensen, R. Bassler, Determination of reinforcement corrosion rate by means of the galvanostatic pulse technique, First International Conference on Bridge Maintenance, Safety and Management IABMAS (2002).
[81] I. García-Lodeiro, A. Palomo, A. Fernández-Jiménez, Alkali–aggregate reaction in activated fly ash systems, Cem. Concr. Res. 37 (2) (2007) 175–183, https://doi.org/10.1016/j.cemconres.2006.11.002.
[82] D.M. Bastidas, A. Fernández-Jiménez, A. Palomo, J.A. González, A study on the passive state stability of steel embedded in activated fly ash mortars, Corros. Sci. 50 (4) (2008) 1058–1065, https://doi.org/10.1016/j.corsci.2007.11.016.
[83] Yuvaraj Dhandapani, Manu Santhanam, Assessment of pore structure evolution in the limestone calcined clay cementitious system and its implications for performance, Cem. Concr. Compos. 84 (2017) 36–47, https://doi.org/10.1016/j.cemconcomp.2017.08.012.
[84] Lipika Rani Bairi, R.P. George, U. Kamachi Mudali, Microbially induced corrosion of D9 stainless steel–zirconium metal waste form alloy under simulated geological repository environment, Corros. Sci. 61 (2012) 19–27, https://doi.org/10.1016/j.corsci.2012.04.019.
[85] Ali Behnood, Kim Van Tittelboom, Nele De Belie, Methods for measuring pH in concrete: a review, Constr. Build. Mater. 105 (2016) 176–188, https://doi.org/10.1016/j.conbuildmat.2015.12.032.
[86] Florian Deschner, Frank Winnefeld, Barbara Lothenbach, Sebastian Seufert, Peter Schwesig, Sebastian Dittrich, Friedlinde Goetz-Neunhoeffer, Jürgen Neubauer, Hydration of Portland cement with high replacement by siliceous fly ash, Cem. Concr. Res. 42 (10) (2012) 1389–1400, https://doi.org/10.1016/j.cemconres.2012.06.009.
[87] Ana María Aguirre-Guerrero, Ruby Mejía-de-Gutiérrez, Maria João Ribeiro Montês-Correia, Corrosion performance of blended concretes exposed to different aggressive environments, Constr. Build. Mater. 121 (2016) 704–716, https://doi.org/10.1016/j.conbuildmat.2016.06.038.
[88] C. Arya, Y. Xu, Effect of cement type on chloride binding and corrosion of steel in concrete, Cem. Concr. Res. 25 (4) (1995) 893–902, https://doi.org/10.1016/0008-8846(95)00080-V.
[89] Barbara Lothenbach, Gwenn Le Saout, Emmanuel Gallucci, Karen Scrivener, Influence of limestone on the hydration of Portland cements, Cem. Concr. Res. 38 (6) (2008) 848–860, https://doi.org/10.1016/j.cemconres.2008.01.002.
[90] S.E. Hussain, S. Al-Saadoun, Effect of tricalcium aluminate content of cement on chloride binding corrosion of reinforcing steel in concrete, ACI Mater. J. 89 (1993) 3–12.
[91] Y.S. Femenias, U. Angst, F. Moro, B. Elsener, Development of a novel methodology to assess the corrosion threshold in concrete based on simultaneous monitoring of pH and free chloride concentration, Sensors 18 (9) (2018) 3101, https://doi.org/10.3390/s18093101.
[92] Agustín Sánchez-Deza, David M. Bastidas, Angel La Iglesia, Jose-María Bastidas, A simple thermodynamic model on the cracking of concrete due to rust formed after casting, ACMM 64 (3) (2017) 335–339, https://doi.org/10.1108/ACMM-11-2015-1602.
[93] S. Reguer, P. Dillmann, F. Mirambet, J. Susini, P. Lagarde, Investigation of Cl corrosion products of iron archaeological artefacts using micro-focused synchrotron X-ray absorption spectroscopy, Appl. Phys. A 83 (2) (2006) 189–193, https://doi.org/10.1007/s00339-006-3506-3.
[94] S. Li, Marine atmospheric corrosion initiation and corrosion products characterization, Doctoral dissertation, University of Hawaii at Manoa, 2010. http://hdl.handle.net/10125/101922
[95] M. Ishii, M. Nakahira, T. Yamanaka, Infrared absorption spectra and cation distributions in (Mn, Fe)3O4, Solid State Commun. 11 (1) (1972) 209–212, https://doi.org/10.1016/0038-1098(72)91162-3.
[96] F. Zhu, D. Persson, D. Thierry, C. Taxen, Formation of corrosion products on open and confined zinc surfaces exposed to periodic wet/dry conditions, Corrosion 56 (12) (2000) 1256–1265, https://doi.org/10.5006/1.3280514.
[97] Shengxi Li, L.H. Hihara, Aerosol salt particle deposition on metals exposed to marine environments: a study related to marine atmospheric corrosion, J. Electrochem. Soc. 161 (5) (2014) C268–C275, https://doi.org/10.1149/2.071405jes.
[98] M. Khachani, A. El Hamidi, M. Halim, S. Arsalane, Non-isothermal kinetic and thermodynamic studies of the dehydroxylation process of synthetic calcium hydroxide Ca (OH) 2, J Mater Environ Sci 5 (2014) 615–624.